JOURNAL OF VIROLOGY, Apr. 2004, p. 4207–4223 Vol. 78, No. 8
0022-538X/04/$08.00+0 DOI: 10.1128/JVI.78.8.4207–4223.2004

Kaposi's Sarcoma-Associated Herpesvirus/Human Herpesvirus 8 Envelope Glycoprotein gB Induces the Integrin-Dependent Focal Adhesion Kinase–Src–Phosphatidylinositol 3-Kinase–Rho GTPase Signal Pathways and Cytoskeletal Rearrangements

Neelam Sharma-Walia, Pramod P. Naranatt, Harinivas H. Krishnan, Ling Zeng, and Bala Chandran*

Department of Microbiology, Molecular Genetics and Immunology, University of Kansas Medical Center, Kansas City, Kansas 66160

Received 13 August 2003/Accepted 17 December 2003

Human herpesvirus 8 (HHV-8; Kaposi's sarcoma-associated herpesvirus) envelope glycoprotein gB possesses an RGD motif, interacts with α3β1 integrin, and uses it as one of the entry receptors. HHV-8 induces the integrin-dependent focal adhesion kinase (FAK), a critical step in the outside-in signaling pathways necessary for the subsequent phosphorylation of other cellular kinases, cytoskeletal rearrangements, and other functions. As an initial step toward deciphering the role of HHV-8 gB-integrin interaction in infection, signal pathways induced by gB were examined. A truncated form of gB without the transmembrane and carboxyl domains (gBΔTM), a gBΔTM mutant form (gBΔTM-RGA) with an RGD-to-RGA mutation, and inhibitors of cellular kinases were used. HHV-8 gBΔTM, but not gBΔTM-RGA, induced FAK phosphorylation in target cells, which was in part dependent on the presence of α3β1 integrin. FAK was critical for the subsequent phosphorylation of Src by gBΔTM, and Src induction was essential for the phosphorylation of phosphatidylinositol 3-kinase (PI-3K). HHV-8 gBΔTM-induced PI-3K was essential for the induction of RhoA and Cdc42 Rho GTPases that was accompanied by the cytoskeletal rearrangements. These gB-induced morphological changes were inhibited by the PI-3K inhibitors. Ezrin, one of the essential elements required to cross-link the actin cytoskeleton with the plasma membrane and to induce the morphological changes, was induced by the Rho GTPases. Inhibition of cellular tyrosine kinases by the brief treatment of cells with 4′,5,7-trihydroxyisoflavone (genistein) blocked the entry of HHV-8 into target cells. These findings suggest that, independently of other viral glycoproteins and via its RGD motif, HHV-8 gB induces integrin-dependent pre-existing FAK–Src–PI-3K–Rho GTPase kinases. Since these signal pathways play vital roles in host cell endocytosis and movement of particulate materials in the cytoplasm, the early stages of HHV-8 gB interaction with host cells may provide a very conducive environment for the successful infection of target cells.

Kaposi's sarcoma (KS)-associated herpesvirus (KSHV) or human herpesvirus 8 (HHV-8) DNA sequences were first identified in KS lesions of AIDS patients (16). Since then, HHV-8 DNA has been detected in all four epidemiologically distinct forms of KS, viz., AIDS KS, classic KS, endemic aggressive KS, and transplantation-associated KS (6, 21, 50, 51). In addition, HHV-8 is also associated with body cavity-based B-cell lymphomas (BCBL) and multicentric Castleman's disease (6, 21, 50, 51). In vivo, HHV-8 DNA and transcripts have been identified in human B cells, macrophages, epithelial cells, endothelial cells, and keratinocytes (6, 21, 50, 51). HHV-8 has also been shown to infect a variety of cell types in vitro, leading to latent infection, including human B cells, endothelial cells, epithelial cells, fibroblast (HFF) cells, and keratinocytes; Chinese hamster ovary (CHO) cells; primary mouse embryonic fibroblast (Du17) cells; owl monkey kidney cells; and baby hamster kidney (BHK-21) cells (5, 21, 33, 43, 50, 51, 56). HHV-8 enters HFF cells by endocytosis and uses clathrin and a low-pH intracellular environment for infectious entry into these cells (2).

The broad cellular tropism of HHV-8 may be in part due to its interaction with the ubiquitous host cell surface heparan sulfate (HS)-like molecules (3). Two virion envelope-associated glycoproteins, gB and gpK8.1A, have been shown to interact with HS molecules (4, 9, 59). Of all of the human and animal herpesviruses sequenced to date, only HHV-8 gB possesses the RGD (Arg-Gly-Asp) amino acid motif (27–29) in the extracellular domain (3, 35, 45). The RGD motif is the minimal peptide region of many proteins known to interact with subsets of host cell surface integrins. Rabbit anti-HHV-8 gB antibodies, RGD peptide, and antibodies against the α3 and β1 integrins and soluble α3β1 integrin inhibited the infection by HHV-8 (5). Expression of human α3 integrins increased the infectivity of the virus in CHO cells (5), and anti-HHV-8 gB antibodies immunoprecipitated the virus-α3-and-β1 complex (5). Radiolabeled virus binding studies suggested that HHV-8 uses the α3β1 integrin as one of the cellular receptors for entry into target cells (5). However, the mechanism by which HHV-8 gB-integrin interaction facilitates virus entry and infection remains to be defined.

Integrins are a family of heterodimeric receptors containing 24 α and 9 β noncovalently associated transmembrane glyco-

* Corresponding author. Mailing address: Department of Microbiology, Molecular Genetics and Immunology, Mail Stop 3029, The University of Kansas Medical Center, 3901 Rainbow Blvd., Kansas City, KS 66160. Phone: (913) 588-7043. Fax: (913) 588-7295. E-mail: bchandra@kumc.edu.

proteins, generating more than 24 known combinations of αβ cell surface receptors (22, 41). Each cell expresses several combinations of αβ integrins, and each αβ combination has its own binding specificity and signaling properties (17, 22, 39, 41, 44, 46, 47, 48, 49, 54). Integrin interactions with extracellular matrix (ECM) proteins mediate a variety of cell functions, such as activation of focal adhesion (FA) kinases (FAKs), activation of cytoskeleton elements, endocytosis, attachment, motility, regulation of gene expression, cell survival, cell cycle progression, cell growth, apoptosis, and differentiation (17, 22, 39, 41, 44, 46, 47, 48, 49, 54). Engagement of integrin by ECM ligands leads to the assembly of integrins, numerous signaling molecules, including FAK, Src, and $p130^{cas}$, and cytoskeletal proteins like talin, paxillin, vinculin, and α-actinin into aggregates on each side of the membrane, creating the formation of well-defined structures known as FAs. FAs link integrins to ECM proteins on the outside and the cytoplasmic actin cytoskeleton on the inside (17, 22, 39, 41, 44, 46, 47, 48, 49, 54).

HHV-8–integrin interactions lead to the phosphorylation of FAK, suggesting that HHV-8 may induce the cellular signaling pathways (5). Within 5 min postinfection (p.i.), in a FAK- and integrin-dependent manner, HHV-8 activated the phosphatidylinositol 3-kinase (PI-3K)–protein kinase Cζ (PKCζ)–MEK–ERK pathway, and rabbit anti-HHV-8 gB antibodies inhibited the virus-induced signaling pathways (33). Early kinetics of this signaling pathway and its activation by UV-inactivated HHV-8 suggested a role for virus binding and/or entry but not viral gene expression in this induction (33). Studies with human α3 integrin-transfected CHO cells and FAK-null Du3 mouse fibroblast cells suggested that the α3β1 integrin and FAK play roles in HHV-8-mediated signal induction (33). Inhibitors specific for PI-3K, PKCζ, MEK, and ERK significantly reduced virus infectivity without affecting virus binding to target cells (33). Preliminary examination of viral DNA entry suggested a role for PI-3K in HHV-8 entry into target cells and a role for PKCζ, MEK, and ERK at a post-viral-entry stage of infection (33). HHV-8 gB also induced target cell adhesions, suggesting the induction of FAK-associated signaling events (58).

This study was undertaken to define the signal pathways induced by gB as a first step in deciphering the mechanism by which integrin-HHV-8 gB interactions facilitate infection and to examine the early events associated with the gB interactions with host cells. A soluble form of gB (gBΔTM) was used to analyze the early events associated with gB interactions with host cells. Here we present several lines of evidence to show that gB, independently of other viral glycoproteins, induces the FAK–Src–PI-3K–Rho GTPase signaling pathway and extensive cytoskeletal rearrangement in target cells. Inhibition of cellular tyrosine kinases blocked virus entry, thus suggesting that gB-induced signal pathways may play roles in the infection of target cells by HHV-8.

MATERIALS AND METHODS

Cells. HFF cells (Clonetics, Walkersville, Md.), human dermal microvascular endothelial cells (HMVEC-d; CC-2543; Clonetics), CHO-K1 (ATCC CCL-61), HHV-8-carrying human B cells (BCBL-1) (43), recombinant GFP (green fluorescent protein)–HHV-8 (GFP–HHV-8–γKSHV.152)-carrying BCBL-1 (GFP–BCBL-1) cells (56), and BJAB cells (HHV-8-negative human B cells) were used in this study. HFF cells were grown in Dulbecco modified Eagle medium (DMEM) (Gibco BRL, Grand Island, N.Y.) supplemented with 10% fetal bovine serum, 2 mM L-glutamine, and antibiotics. HMVEC-d cells were maintained in endothelial cell growth medium supplemented with growth factors (Clonetics). BJAB cells were grown in RPMI 1640 medium (Gibco BRL). Primary mouse embryonic fibroblasts null for FAK (Du3), control FAK-wild-type (wt) Du17 cells (gifts from D. Ilic, University of California at San Francisco) were grown as described earlier (24). CHO-B2 cells transfected with pCDNA3 (CHO-B2/pCDNA) and human α3 integrin cDNA containing pCDNA3 (CHO-B2 clone B3; gifts from J. A. McDonald, Samuel C. Johnson Medical Research Center, Mayo Clinic, Scottsdale, Ariz.) were grown as described previously (61). All cells were grown in lipopolysaccharide (LPS)-free medium.

Antibodies and reagents. Mouse anti-phosphotyrosine (PY20) antibodies were obtained from Calbiochem, La Jolla, Calif. Polyclonal rabbit immunoglobulin G (IgG) antibodies against PI-3K p85α (Z-8), phospho-ezrin (Tyr146), RhoA (110), Rac (C14), Cdc42 (P1), and epidermal growth factor (EGF) receptor (EGFR) were from Santa Cruz Biotechnology, Inc., Santa Cruz, Calif. Mouse anti-phospho-FAK antibodies (Y397) were from BD Biosciences, San Jose, Calif. Anti-Src (PY418) and anti-Src (total) antibodies and tyrosine kinase assay kits were obtained from Upstate Biotechnology, Lake Placid, N.Y. LY294002 [20(4-morphodinyl)-8-phenyl-1(4H)-benzopyran-4-one], leupeptin, aprotinin, wortmannin, lysophosphatidic acid (LPA), EGF, rabbit anti-pp125 FAK antibodies, and monoclonal antibodies (MAb) against β-actin (CloneAC-40), genistein, and tubulin were from Sigma, St. Louis, Mo. Purified soluble α3β1 and α5β1 integrins (*n*-octylpyranoside preparation) were from Chemicon International, Temecula, Calif. Anti-rabbit and anti-mouse antibodies linked with horseradish peroxidase (HRP), fluorescein isothiocyanate (FITC), or TRITC (tetramethyl rhodamine isothiocyanate) were from Kirkegaard & Perry Laboratories, Inc., Gaithersburg, Md. Protein A–Sepharose CL-4B beads were from Amersham Pharmacia Biotech, Piscataway, N.J. Protein tyrosine phosphatase 1B, SU6656, PP2, tyrphostin, and C3 exotoxin were from Calbiochem. The CNM compartment protein extraction kit was obtained from the Biochain Institute, Inc., Hayward, Calif.

Expression of recombinant HHV-8 gBΔTM and gBΔTM-RGA proteins. The generation and purification of recombinant baculovirus-expressed gBΔTM, gBΔTM-RGA, and ΔTMgpK8.1A proteins have been described before (58, 59, 62). Recombinant protein purifications were done with buffers prepared with LPS-free water, and stock preparations of proteins were monitored for endotoxin contamination by standard *Limulus* assay (Limulus Amebocyte Lysate Endochrome; Charles River Endosafe, Charleston, S.C.) as recommended by the manufacturer.

Rabbit anti-gB antibodies. The generation of rabbit polyclonal antibodies against full-length HHV-8 gB and gBΔTM and against gB peptides (gB-N1, gB-N2, gB-N3, and gB-C) has been described before (58). IgG fractions were purified with protein A-Sepharose 4B columns, and the nonspecific antibodies were removed with columns of cyanogen bromide-activated Sepharose 4B covalently coupled with purified glutathione *S*-transferase protein and BJAB-cell lysate.

Cytotoxicity assays. Target cells were incubated with different concentrations of recombinant proteins at 37°C for different times (5, 15, 30, and 60 min). Supernatants were collected and assessed by cytotoxicity assay kit (Promega, Madison, Wis.) in accordance with the manufacturer's recommendations. Viability of cells was also tested by trypan blue exclusion test.

Measurement of FAK phosphorylation at Tyr^{397}. Target cells grown to 80% confluence in T25 flasks were serum starved by incubation with DMEM at 37°C for 24 h. These cells were incubated with DMEM or with DMEM containing various concentrations of gBΔTM, gBΔTM-RGA, or ΔTMgpK8.1A for different times (5, 10, 15, 30, 60, and 120 min) at 37°C. Experiments were also performed with cells that were pretreated with tyrosine kinase inhibitors (genistein [4′,5,7-trihydroxyisoflavone] and tyrphostin) for 1 h at 37°C prior to the addition of various recombinant proteins. In another set of experiments, recombinant proteins were preincubated with anti-gB antibodies or integrins for 1 h at 37°C before addition to the cells. Cells were lysed on ice for 20 min by addition of 0.5 ml of radioimmunoprecipitation assay (RIPA) lysis buffer (1% Nonidet P-40, 1% sodium deoxycholate, 0.1% sodium dodecyl sulfate [SDS], 125 mM NaCl, 0.01 M sodium phosphate [pH 7.2], 1 mM EDTA, 1 mM phenylmethylsulfonyl fluoride, 500 μg of leupeptin per ml, 0.2 mM sodium orthovanadate [Na_3VO_4], 50 mM sodium fluoride, 100 μl of aprotinin per 25 ml). Cell debris and nuclei were removed by centrifugation at 13,000 × *g* for 20 min at 4°C, and the supernatant was frozen at −80°C. The protein concentration of the clarified supernatant was determined with a micro-BCA (bicinchoninic acid) protein assay kit (Pierce, Rockford, Ill.). Each sample was heated at 95°C for 5 min, resolved by SDS–10% polyacrylamide gel electrophoresis (PAGE), transferred to nitrocellulose membranes, and blocked in 5% bovine serum albumin (BSA) in TBST (150 mM NaCl, 10 mM Tris-HCl [pH 7.2]) with 0.02% NaN_3. Phosphorylated FAK content was assessed by immunoblotting with anti-phospho-FAK antibody (Y397).

To confirm equal protein loading, membranes were stripped and reprobed with goat anti-rabbit pp125 FAK and anti-β-actin antibodies. Immunoreactive bands were visualized by development with the enhanced-chemiluminescence reaction (ECL; NEN Life Sciences Products, Boston, Mass.). Bands were scanned and quantitated with the ImageQuant software program (Molecular Dynamics). The phosphotyrosine residue in FAK was dephosphorylated by incubating the cell lysate with 0.5 U of protein tyrosine phosphatase 1B (Calbiochem) for 3 h at 30°C before testing with anti-FAK antibodies.

Measurement of Src kinase phosphorylation. Serum-starved target cells were stimulated with various concentrations of ligands and inhibitors. Cells were also incubated with the kinase inhibitors tyrphostin (50 or 100 μM), genistein (100 μM), PP2 (4 μM), and SU6656 (2 μM) for 1 h at 37°C or with the PI-3K inhibitors wortmannin (100 nM) and LY294002 (20 μM) and then treated with gBΔTM at 37°C in the presence of inhibitors. Cells were lysed in RIPA lysis buffer containing protease inhibitor cocktail. Cell debris and nuclei were removed by centrifugation at 13,000 × *g* for 20 min at 4°C, and the supernatant was frozen at −80°C. This supernatant was precleared with 30 μl of Zysorbin (fixed and killed *Staphylococcus aureus* protein A-positive strain) per ml for 30 min at 4°C, and the protein concentration was determined with a micro-BCA protein assay kit (Pierce). Each sample was heated at 95°C for 5 min, resolved by SDS–7.5% PAGE, transferred on nitrocellulose membranes, and probed with anti-Src (PY418) antibody for 3 h. Immunoreactive bands were visualized with an HRP-conjugated secondary antibody and quantitated as described above. Equal protein loading was confirmed by stripping the membranes and reprobing with anti-Src (total) antibody.

Src kinase activities were also measured with a nonradioactive two-step peptide phosphorylation-colorimetric kinase detection assay kit (Upstate Biotechnology) as recommended by the manufacturer. In the first stage, a biotinylated substrate peptide containing tandem repeats of poly(Glu_4-Tyr) is incubated with a tyrosine kinase enzyme sample in the presence of nonradioactive ATP and an Mn^{2+}-Mg^{2+} cofactor cocktail. The kinase assay was performed with substrate peptide in a solution used to coat the surface of a streptavidin-coated 96-well plate. The second step involved detection of the phosphorylated substrate by direct enzyme-linked immunosorbent assay with anti-phosphotyrosine–HRP MAb and a tetramethylbenzidine substrate.

Measurement of PI-3K induction. Serum-starved target cells were stimulated with various concentrations of recombinant proteins and inhibitors. Cells were also incubated with the PI-3K inhibitors wortmannin (100 nM) and LY294002 (20 μM) for 1 h at 37°C and then incubated with gBΔTM at 37°C in the presence of inhibitors. Cells were lysed in RIPA lysis buffer containing a protease inhibitor cocktail. Cellular debris was removed by centrifugation at 13,000 × *g* for 20 min at 4°C. Clarified supernatants were precleared with Zysorbin, and the protein concentration was determined. The catalytic complex of PI-3K was immunoprecipitated from 500 μg of ice-cold precleared supernatant by incubation with anti-phosphotyrosine MAb PY20 for 2 h at 4°C. Immune complexes were washed four times with ice-chilled RIPA buffer containing protease inhibitors, and the bound proteins were eluted by boiling in 50 μl of 2× Laemmli buffer for 3 min. The insoluble material was removed by centrifugation, and the supernatant was subjected to Western blot analysis. The nitrocellulose membrane was probed with PI-3K p85α (Z-8) antibody for 2 h at room temperature and washed, and the immunoreactive bands were visualized with an HRP-conjugated secondary antibody and quantitated by ECL as described above. The total p85 (PI-3K) level was measured by testing the whole-cell lysate in Western blot assays with PI-3K p85α (Z-8) antibody. Actin was used as a loading control.

Measurement of Rho GTPase activation. Serum-starved target cells were treated with gBΔTM for various times. Cells were also incubated with 30 μg of C3 exotoxin per ml for 12 h before incubation with the proteins. These cells were rinsed twice with ice-cold phosphate-buffered saline (PBS), trypsinized, pelleted, and fractionated into cytosolic, membrane, and nuclear fractions with the CNM compartment protein extraction kit as recommended by the manufacturer. The membrane and cytosolic fractions were checked for specificity by Western blotting with anti-EGFR and anti-tubulin antibodies, respectively. These fractions were separated by SDS–12.5% PAGE, and the RhoA, Rac, and Cdc42 proteins were detected by Western blot analysis with RhoA-, Rac-, and Cdc42-specific antibodies.

Measurement of ezrin activation. Serum-starved HFF cells were incubated with various ligands for different time. Cells were also incubated with 30 μg of C3 exotoxin per ml for 12 h before incubation with the ligands. All cell lysates were resolved by SDS–10% PAGE and tested by Western blot analyses with anti-phospho-ezrin antibody. Immunoreactive bands were visualized with an HRP-conjugated secondary antibody and quantitated as described above.

Fluorescence microscopic observation of morphological changes and actin polymerization. HFF cells in eight-well chamber slides (75% confluence) were serum starved for 24 h, washed twice with PBS, and then treated with 1 μg of gBΔTM or gBΔTM-RGA per ml or with EGF (100 ng/ml) for different lengths of time. Cells were also preincubated with a PI-3K inhibitor (LY294002; 20 μM) for 1 h at 37°C and then treated with EGF (100 ng/ml) or gBΔTM (1 μg/ml) for 30 min in the presence of inhibitors. At respective time points, cells were washed with PBS, fixed with 3.7% formaldehyde in PBS for 10 min, washed, permeabilized with 0.1% Triton X-100 in PBS for 3 min, and blocked with 1% BSA in PBS for 10 min at room temperature. These cells were incubated for 20 min at room temperature with rhodamine-labeled phalloidin (Molecular Probes, Eugene, Oreg.) in PBS, washed, and examined under a fluorescence microscope.

Colocalization of ezrin and actin by immunofluorescence. Serum-starved HFF cells in eight-well chamber slides were treated with 1 μg of gBΔTM per ml for 15 min at 37°C. Treated and untreated cells were washed in PBS for 10 min at room temperature and incubated with 3.7% formaldehyde in PBS. Cells were permeabilized with 0.1% Triton X-100–PBS for 3 min, blocked with 1% BSA–PBS for 10 min at room temperature, washed, and incubated with anti-phospho-ezrin antibody for 30 min at room temperature. These cells were washed with PBS, incubated with the respective FITC-conjugated secondary antibodies for 30 min at room temperature, washed in PBS, and stained with rhodamine-labeled phalloidin for 20 min at room temperature. Stained cells were washed and viewed with appropriate filters under a fluorescence microscope with the Nikon Magna Firewire digital imaging system.

Measurement of GFP–HHV-8 infection. Effects of protein kinase inhibitors on HHV-8 were measured by using GFP–HHV-8–γKSHV.152 as described before (5, 33). Briefly, HFF cells were incubated at 37°C for 1 h with and without protein kinase inhibitors in DMEM, infected with GFP–HHV-8 in the presence or absence of inhibitors at 37°C for 2 h, washed twice with DMEM, and further incubated with growth medium at 37°C. After 3 days, infection was monitored by counting the green fluorescent cells (5, 33).

Measurement of HHV-8 internalization by real-time DNA PCR. Effects of protein kinase inhibitors on HHV-8 internalization were assessed by real-time DNA PCR detecting the internalized HHV-8 DNA as described before (32). Briefly, viral DNA was extracted from purified HHV-8 and the copy numbers were quantitated by real-time DNA PCR with primers amplifying the HHV-8 open reading frame 73 (ORF73) gene (25). Untreated HFF cells or HFF cells incubated with inhibitors for 1 h at 37°C were infected with HHV-8 at 10 DNA copies/cell. After 2 h of incubation, cells were washed twice with PBS to remove the unbound virus, treated with trypsin-EDTA for 5 min at 37°C to remove the bound but noninternalized virus, and washed, and total DNA was isolated with a DNeasy kit (Qiagen, Valencia, Calif.). One hundred nanograms of DNA samples, HHV-8 ORF73 gene TaqMan probe (25), and Quantitect PCR mix was used. The HHV-8 ORF73 gene cloned into the pGEM-T vector (Promega) was used for the external standard. Known amounts of ORF73 plasmid were used in the amplification reaction mixtures along with the test samples. The lower limit of ORF73 gene detection was 10 to 100 copies, and the most accurate detection was from 100 to 10^6 copies. Special care was taken to keep the slope of the standard curve close to 3.3 so that the amplification efficiency of the cycles was 2 (20). The threshold cycle (Ct) values were used to plot the standard graph and to calculate the relative copy numbers of viral DNA in the samples.

Measurement of HHV-8 gene expression by real-time RT-PCR. Effects of protein kinase inhibitors on HHV-8 viral gene expression were assessed by real-rime reverse transcriptase PCR (RT-PCR) detecting HHV-8 ORF73, and gene expression was carried out as described before (32). Briefly, untreated HFF cells or HFF cells incubated with inhibitors for 1 h at 37°C were infected with HHV-8 at 10 DNA copies/cell. After 2 h of incubation, total RNA was isolated from the cell lysate with RNeasy kits (Qiagen) in accordance with the manufacturer's protocols, quantified, and treated with DNase I, and HHV-8 ORF50 and ORF73 transcripts were detected by real-time RT-PCR with gene-specific TaqMan probes (25). Known concentrations of gene-specific transcripts from the cloned genes were used as external control samples. All samples were used in separate real-time DNA PCRs (without RT) to confirm the absence of contaminating DNA. The relative copy numbers of the transcripts were calculated from the standard graph plotted with the Ct values for different dilutions of in vitro-transcribed transcripts. These values were normalized to each other with the values of glyceraldehyde-3-phosphate dehydrogenase (GAPDH) control reactions. The number of GAPDH transcripts in each sample was calculated from the standard graph plotted with copy numbers from different dilutions of the known concentrations of human RNA and TaqMan GAPDH reagents. The standard graph of the external control reactions was used to determine the relative copy numbers of respective transcripts in each sample, while the GAPDH control reaction was used to normalize the amount of initial template in each reaction. The lower limit of detection in the standard samples was 10 to 100 copies of

transcripts for both the ORF50 and ORF73 genes, while copy numbers in the range of 100 to 10^6 were detected with more accuracy. As in the real-time DNA PCR, maximum care was taken to keep the slope of the standard curve close to 3.3.

RESULTS

HHV-8 gBΔTM induces the phosphorylation of FAK at Tyr^{397}. FAK is a cytoplasmic nonreceptor tyrosine kinase, and FAK activation is the first step necessary for the outside-in signaling by integrins (22, 46, 47, 48, 49). FAK activation and tyrosine phosphorylation in a variety of cell types have been shown to be dependent on integrins binding to their extracellular ligands (13, 14, 17, 22, 46, 47, 48), and in adherent cells, FAK colocalizes with integrins in focal contacts. Following integrin-ligand interaction, FAK is autophosphorylated at Tyr^{397} residue, which is critical for the subsequent phosphorylation of other FA proteins (13, 17, 22, 47, 49). Tyr^{397} is the primary site of FAK phosphorylation, as well as the initiation of further FAK activation, since it is the binding site for the SH2 domain of Src family kinases. These interactions link FAK to the signaling pathways that modify the cytoskeletal rearrangement and activate the mitogen-activated protein kinase cascades (22, 47, 49).

We have previously shown that as early as 5 min p.i. of HFF cells, purified HHV-8 induced the phosphorylation of FAK (5). To characterize the FAK activation by HHV-8 gB in detail, we used the baculovirus-expressed recombinant gBΔTM and gBΔTM-RGA proteins, which were purified and characterized as described before (58, 59). Serum-starved HFF cells were treated with various ligands at 37°C, and phosphorylation of FAK at Tyr^{397} was assessed by immunoblot assays with anti-phospho-FAK antibodies. Compared to the uninduced cells, FAK phosphorylation increased about 10-fold when cells were treated with 20 ng of LPA for 5 min (Fig. 1A, top, lanes 1 and 2). Similarly, incubation of cells with increasing concentrations of gBΔTM for 30 min rapidly induced the phosphorylation of FAK, with about 1.2-, 2-, 6-, and 9-fold FAK phosphorylation activity over control cells by 0.25, 0.5, 1, and 2 μg of gBΔTM per ml, respectively (Fig. 1A, top, lanes 3 to 6). To confirm equal protein loading, membranes were stripped and reprobed with rabbit anti-pp125 FAK and mouse anti-β-actin antibodies. Equal amounts of total FAK and actin were detected in all of the samples (Fig. 1A, middle and bottom, respectively), demonstrating the steady-state level of endogenous FAK. These results suggested that gBΔTM was activating pre-existing FAK.

Treatment of HFF cells with 4-, 8-, 16-, and 32-μg/ml concentrations of gBΔTM resulted in loss of FAK phosphorylation (Fig. 1A, top, lanes 7 to 10). To determine the cause of this, we examined the effects of gBΔTM on the viability of HFF cells. In cells treated with 8, 16, and 32 μg of gBΔTM per ml, significant morphological changes such as rounding and detachment, as well as loss of viability, were observed. More than 50% cell death was observed at a 32-μg/ml concentration (data not shown). No significant morphological changes were observed in cells incubated with the gBΔTM-RGA and ΔTMgpK8.1A proteins, even at a concentration of 32 μg/ml (data not shown). These results suggested that the reduced FAK phosphorylation by the physiologically nonrelevant high concentrations of gBΔTM could be due to a toxic effect. Hence, in all subsequent experiments, we used only the nontoxic lower concentrations of proteins.

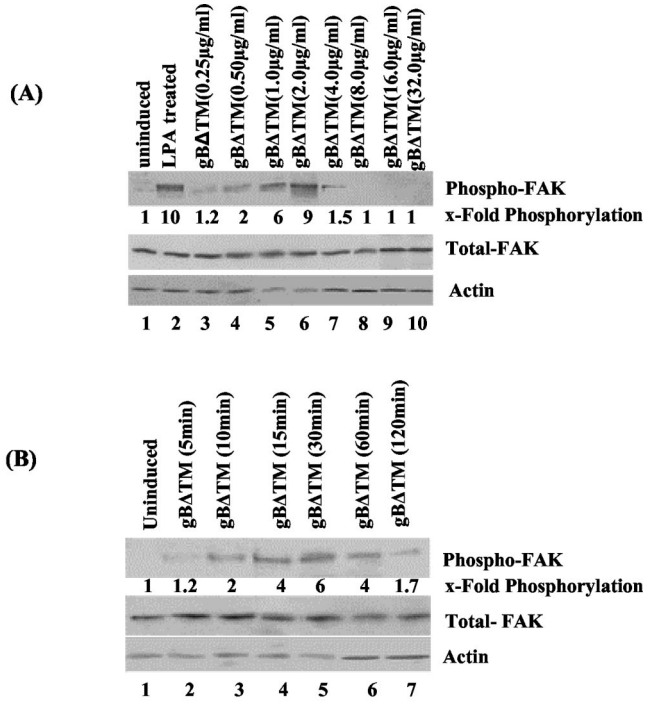

FIG. 1. HHV8 gBΔTM activates the phosphorylation of FAK in HFF cells. (A, top) Serum-starved HFF cells were left uninduced (lane 1), induced with 20 ng of LPA for 5 min (lane 2), or induced with 0.25, 0.5, 1.0, 2.0, 4.0, 8.0, 16.0, and 32.0 μg of gBΔTM protein per ml (lanes 3, 4, 5, 6, 7, 8, 9, and 10, respectively) at 37°C for 30 min. Cells were lysed, and cell debris and nuclei were removed. Equal amounts of supernatant were resolved by SDS–10% PAGE, Western blotted, and reacted with mouse anti-phospho-FAK antibodies (Y397). Immunoreactive bands were visualized by the enhanced-chemiluminescence reaction, and band intensities were assessed. (A, middle and bottom) After reactions, membranes in the top part were stripped and reprobed with anti-pp125 FAK and anti-β-actin antibodies, respectively. Each blot is a representative of at least three independent experiments. FAK phosphorylation in uninduced cells was assigned a value of 1 for comparison, and the values shown are fold increases in the phosphorylation of FAK in induced cells. Each point represents the average ± the standard deviation of three independent experiments. (B, top) Serum-starved HFF cells were left uninduced (lane 1) or treated with 1 μg of gBΔTM protein per ml at 37°C for 5, 10, 15, 30, 60, and 120 min (lanes 2 to 7, respectively). At the end of the incubation period, cells were processed and FAK phosphorylation was measured and quantitated as described for panel A. (B, middle and bottom) After reactions, membranes in the top part were stripped and reprobed with anti-pp125 FAK and anti-actin antibodies, respectively. Each blot is representative of at least three independent experiments. FAK phosphorylation induced by gBΔTM was expressed as increased phosphorylation of FAK over that of uninduced cells, which was assigned a value of 1. Each point represents the average ± the standard deviation of three experiments.

Kinetics of FAK phosphorylation by HHV-8 gBΔTM. A time-dependent increase in the phosphorylation of FAK was observed when HFF cells were incubated with 1.0 μg of gBΔTM per ml for different times at 37°C (Fig. 1B). By 10 min post gBΔTM incubation, FAK phosphorylation increased twofold over the uninduced control cells, steadily increased over time, reached a peak by 30 min, and decreased thereafter.

FAK phosphorylation increased by 1.2-, 2-, 4-, 6-, 4-, and 1.7-fold in cells incubated with gBΔTM for 5, 10, 15, 30, 60, and 120 min, respectively (Fig. 1.B, top, lanes 1 to 7). The expression levels of total FAK and actin were maintained at the same level (Fig. 1A, middle and bottom, respectively), demonstrating that gBΔTM was activating pre-existing FAK.

Specificity of FAK phosphorylation by HHV-8 gBΔTM. We have previously demonstrated that gBΔTM mediated the adhesion of three different target cells, which was abolished by a single amino acid change from RGD to RGA (58). HHV-8 gpK8.1A is a 228-amino-acid virion envelope-associated glycoprotein, and it interacts with cell surface HS molecules (4, 9, 59, 62). The specificity of FAK phosphorylation by gBΔTM was shown by the absence of FAK activation in HFF cells incubated for 30 min with 1 μg of ΔTMgPK8.1A and gBΔTM-RGA per ml (Fig. 2A, top, lanes 1, 2, and 3). In contrast, as seen before, 1 μg of gBΔTM per ml induced FAK phosphorylation sixfold (Fig. 2A, top, lane 4). FAK activity induced by gB was lowered to the background level when the samples after 30 min with gBΔTM were incubated with 0.5 U of protein tyrosine phosphatase 1B for 3 h at 30°C to dephosphorylate the phosphotyrosine residue (Fig. 2A, top, lane 5). These results demonstrated the specificity of anti-phospho-FAK antibodies and suggested that FAK phosphorylation by gB was mediated by its RGD motif. PI-3K is one of the important downstream effector molecules of FAK phosphorylation, and HHV-8 has been shown to induce PI-3K within 5 min after infection (33). To verify the specificity of FAK activation further, cells were incubated with the PI-3K inhibitor LY294002 (20 μM) for 1 h at 37°C before incubation with 1 μg of gBΔTM per ml in the presence of LY294002. No effect on the phosphorylation of FAK was seen (Fig. 2A, top, lane 6). This suggested that FAK is an upstream mediator of PI-3K and demonstrated the specificity of FAK activation.

Genistein is a tyrosine kinase-competitive inhibitor of the ATP binding site (1) and inhibits several tyrosine kinases, including FAK, as well as the assembly of FAs (13, 17, 22, 46, 47, 49). Incubation of cells with 140 μM genistein has been shown to inhibit the integrin-induced signaling and cytoskeletal protein complexes without profound cytotoxicity (47). Treatment of cells for 1 h with predetermined nontoxic concentrations of 100, 50, and 25 μM genistein and 30 min of incubation with gBΔTM lowered the gBΔTM-induced phosphorylation of FAK from sixfold to one-, four-, and sixfold, respectively (Fig. 2A, top, lanes 7 to 9). Dimethyl sulfoxide, which was used as a solvent for genistein, did not alter the expression of FAK (data not shown).

Tyrphostin is a member of the AG compound family, structurally resembling tyrosine and erbstatin moieties with hydrophobic characteristics, allowing it to traverse the cell membrane and inhibit protein tyrosine kinases by binding to the substrate binding site (37). HHV-8 gB-induced FAK activity in HFF cells (sixfold) was reduced to one- and fivefold by nontoxic doses of 100 and 50 μM tyrphostin, respectively (Fig. 2A, top, lanes 10 and 11). In all of these experiments, the levels of total FAK and actin did not change (Fig. 2A, middle and bottom, respectively), thus demonstrating that gBΔTM was phosphorylating pre-existing FAK.

To further ascertain the specificity of FAK activation, anti-gB IgG antibodies were incubated with gBΔTM for 1 h at 37°C before addition to HFF cells. Incubation with 25, 50, and 100 μg of anti-gB antibodies per ml reduced FAK phosphorylation by 20, 60, and 80%, respectively (Fig. 2B, top, lanes 2, 3, and 4). No inhibition was obtained with 100 μg of preimmune IgG antibodies per ml (Fig. 2B, top, lane 5). To determine whether gB-FAK activation is a cell type-specific phe-

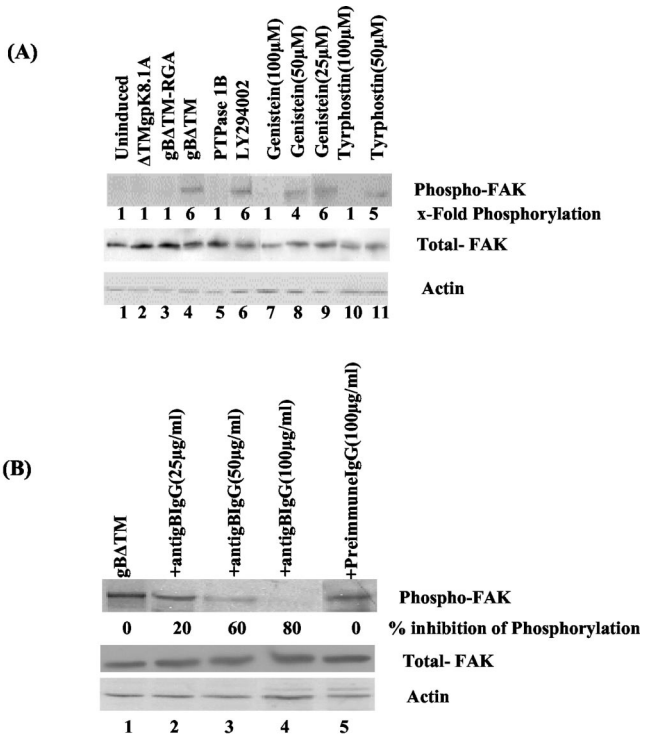

FIG. 2. Specificity of HHV-8 gBΔTM-induced FAK phosphorylation. (A, top) Lanes: 1, uninduced, serum-starved HFF cells; 2, 3, and 4, cells induced with 1 μg of ΔTMgPK8.1A, gBΔTM-RGA, and gBΔTM proteins per ml, respectively; 5, cells treated with gBΔTM at 37°C and dephosphorylated by incubating the membranes with 0.5 U of protein tyrosine phosphatase 1B for 3 h at 30°C before reaction with anti-FAK antibodies; 6, cells incubated with the PI-3K inhibitor LY294002 (20 μM) for 1 h at 37°C and then treated with gBΔTM at 37°C in the presence of the inhibitor; 7, 8, and 9, cells treated with 100, 50, and 25 μM concentrations of genistein, respectively, for 1 h at 37°C and then treated with gBΔTM at 37°C in the presence of genistein; 10 and 11, cells treated with 100 and 50 μM concentrations of tyrphostin, respectively, for 1 h at 37°C and then treated with gBΔTM at 37°C in the presence of tyrphostin. At the end of the 30-min period of incubation with proteins at 37°C, cells were processed and FAK phosphorylation was quantitated as described in the legend to Fig. 1A. (A, middle and bottom). After reactions, membranes in the top part were stripped and reprobed with anti-pp125 FAK and anti-β-actin antibodies, respectively. Each blot is representative of at least three independent experiments. (B, top) Lanes: 1, serum-starved HFF cells induced with gBΔTM at 37°C; 2, 3, and 4, gBΔTM preincubated with 25, 50, and 100 μg of anti-gB IgG antibodies per ml, respectively, before addition to cells; 5, gBΔTM preincubated with 100 μg of preimmune IgG antibodies per ml before addition to cells. Cells were processed and FAK phosphorylation was measured as described for panel A. (B, middle and bottom) After reactions, membranes in the top part were stripped and reprobed with anti-pp125 FAK and anti-β-actin antibodies, respectively. Each blot is representative of at least three independent experiments. Data are presented as a percentage of the inhibition of FAK phosphorylation obtained when the cells were incubated with the gBΔTM protein only.

nomenon, FAK activation was tested in HMVEC-d cells. The basal level of FAK activation in unstimulated HMVEC-d cells is much higher (2.5-fold) than that in HFF cells, and treatment of HMVEC-d cells with gBΔTM induced FAK phosphorylation about sixfold (data not shown). Taken together, these results demonstrated the specificity of HHV-8 gB phosphorylation of FAK.

HHV-8 gBΔTM interaction with α3β1 induces FAK phosphorylation. Our studies have shown that HHV-8 uses the cell surface α3β1 integrin as one of the entry receptors, induces FAK phosphorylation as early as 5 min p.i., and was inhibited by virus preincubation with soluble α3β1 integrin and anti-gB antibodies (5). To determine the role of gBΔTM-α3β1 integrin interaction in FAK activation independently of other viral glycoproteins, soluble α3β1 and α5β1 integrins were mixed with gBΔTM (1 μg/ml) and incubated for 1 h at 37°C before addition to HFF cells and incubation for 30 min. Incubation with 5.0, 2.5, and 1.25 μg of soluble α3β1 integrin per ml lowered FAK phosphorylation by 67, 59, and 13%, respectively (Fig. 3A, top, lanes 1 to 4). In contrast, 5.0 μg of α5β1 per ml did not inhibit FAK phosphorylation (Fig. 3A, top, lane 5). The levels of total FAK and actin did not change (Fig. 3A, middle and bottom, respectively). These results not only demonstrated the specificity of FAK activation by gB but also suggested that gB interaction with α3β1 is one of the critical elements required for the observed FAK induction.

To verify further the role of α3β1 in gBΔTM-mediated FAK induction, we used CHO-B2 cells expressing low levels of endogenous α3 integrin and human α3 integrin cDNA-transfected CHO-B2 clone B3 cells (5, 61). The human α3 integrin formed heterodimeric complexes with hamster β1, and more than 95% of the CHO-B2 clone B3 cells expressed human α3 integrin on their surfaces (5, 61). The efficiency of infection in CHO-B2 cells was about 25-fold less than that in HFF and HMVEC-d cells. However, CHO-B2 clone B3 cells were two to three times more susceptible to HHV-8 infectivity than were parental CHO-B2 cells, confirming the role of α3β1 integrin in HHV-8 infectivity (5). Compared to that of unstimulated cells, incubation of CHO-B2 cells with gBΔTM resulted in about 2.5-fold activation of FAK (Fig. 2B, top, lanes 1 and 2) and that of CHO-B2 clone B3 cells resulted in about 6-fold activation (Fig. 2B, top, lanes 3 and 4). The levels of total FAK and actin did not change (Fig. 3B, middle and bottom, respectively). Activation of FAK in CHO-B2 cells could be due to gB interaction with hamster α3β1 and other integrins. Since the expression of human α3 integrin increased the phosphorylation of FAK in CHO-B2 clone B3 cells, these results also support the notion that gBΔTM interaction with α3β1 integrin is one of the essential elements required for induction of FAK.

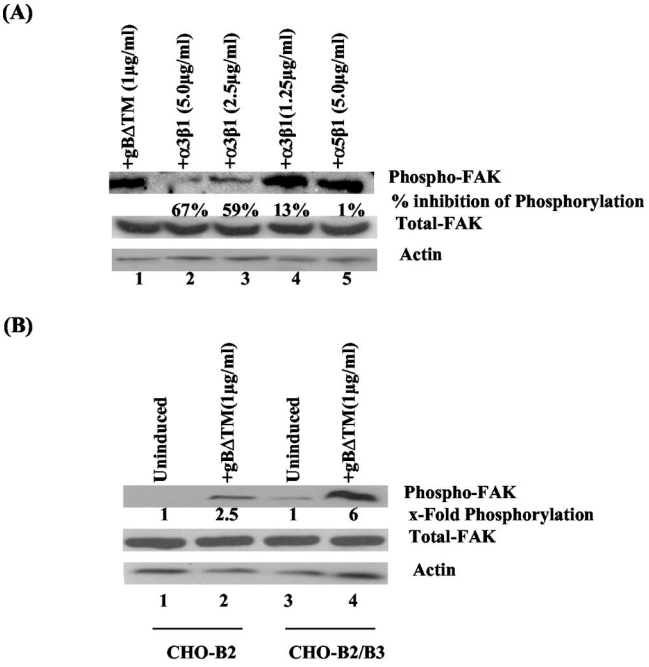

FIG. 3. Integrin α3β1 is one of the essential elements required for FAK induction by HHV-8 gBΔTM. (A, top) Soluble α3β1 or α5β1 integrin was mixed with 1 μg of gBΔTM per ml for 1 h at 37°C before incubation with serum-starved HFF cells at 37°C for 30 min. Lanes: 1, cells induced with 1 μg of gBΔTM per ml; 2, 3, and 4, gBΔTM preincubated with 5, 2.5, and 1.25 μg of soluble α3β1 per ml, respectively; 5, gBΔTM preincubated with soluble α5β1 integrin. Cells were processed and FAK phosphorylation was measured as described in the legend to Fig. 1A. (A, middle and bottom) After reactions, membranes in the top part were stripped and reprobed with anti-pp125 FAK and anti-β-actin antibodies, respectively. Each blot is representative of at least three independent experiments. FAK phosphorylation was quantitated as described in the legend to Fig. 1A. Data are presented as a percentage of the inhibition of FAK phosphorylation obtained when the cells were incubated with the gBΔTM protein only. Each point represents the average ± the standard deviation of three experiments. (B) Serum-starved CHO-B2 cells expressing low levels of endogenous α3 integrin transfected with control plasmid pCDNA3 and CHO-B2 clone B3 cells transfected with pCDNA3-human α3 integrin cDNA were used to assess the activation of FAK. (Top) Lanes: 1, uninduced CHO-B2 cells; 2, gBΔTM-induced CHO-B2 cells; 3, uninduced CHO-B2 clone B3 cells; 4, gBΔTM-induced CHO-B2 clone B3 cells. (Middle and bottom) After reactions, membranes in the top part were stripped and reprobed with anti-pp125 FAK and anti-β-actin antibodies, respectively. Each blot is representative of at least three independent experiments. FAK phosphorylation was quantitated as described in the legend to Fig. 1A and expressed as the fold increase in phosphorylation of FAK over that of uninduced cells (assigned a value of 1). Each point represents the average ± the standard deviation of three experiments.

HHV-8 gBΔTM induces phosphorylation of Src. Autophosphorylation at the Tyr^{397} residue of FAK leads to binding of the SH2 domain of Src family kinases (13, 22, 29, 47, 48, 49, 54). The Src family of tyrosine kinases, including Src, Lyn, Fyn, Yes, Lck, Blk, and Hck, plays critical roles in various signal transduction pathways, and these tyrosine kinases are important regulators of growth and differentiation in eukaryotic cells. The expression of Src family members differs according to the cell type, and Src activity is regulated by tyrosine phosphorylation at two sites with opposing effects (29, 47, 48, 54). Phosphorylation of Tyr^{418} in the activation loop of the kinase domain upregulates the enzyme, and phosphorylation of Tyr^{527} in the C-terminal tail by the cytosolic protein tyrosine kinase Csk (carboxy-terminal Src kinase) renders the enzyme less active (14, 15, 22, 47). After the Src-SH2 domain binds to FAK-Tyr^{397}, activated Src kinases then phosphorylate a number of FA components (14, 15, 22, 47).

Since HHV-8 gB induced a robust FAK response in target cells, we next examined the ability of gB to induce Src kinase activity. Treatment of HFF cells with EGF and LPA, which were used as positive controls, induced the Src kinases by

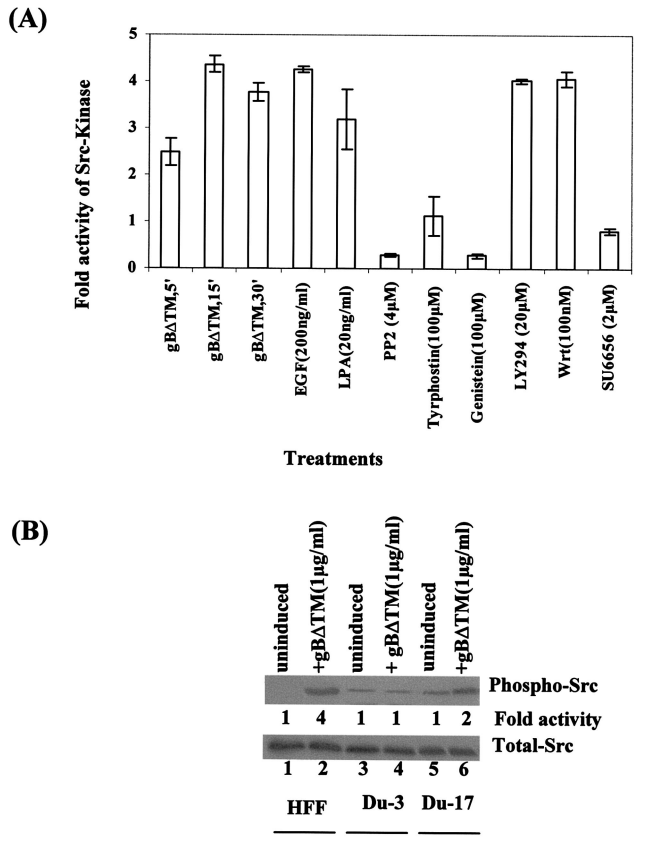

FIG. 4. HHV-8 gBΔTM induces phosphorylation of Src at Tyr^{418}. (A) Quantitation of Src kinase activity induced by gBΔTM in HFF cells. Serum-starved HFF cells were left uninduced or induced with EGF (200 ng/ml) for 15 min, with LPA (20 ng/ml) for 5 min, or with 1.0 μg of gBΔTM per ml for 5, 15, and 30 min at 37°C. Cells were also treated with nontoxic doses of tyrphostin (100 μM), genistein (100 μM), PP2 (4 μM), SU6656 (2 μM), wortmannin (100 nM), and LY294002 (20 μM) for 1 h at 37°C and then incubated with gBΔTM at 37°C for 30 min in the presence of inhibitors. Src kinase activities were measured with a nonradioactive two-step peptide phosphorylation-colorimetric kinase detection assay kit. Src kinase activity in uninduced HFF cells was assigned a value of 1 for comparison. Each point represents the average ± the standard deviation of three experiments. (B) Serum-starved FAK-null Du3, FAK-wt Du17, and HFF cells were stimulated with gBΔTM at 1 μg/ml at 37°C for 30 min. Cells were lysed, and samples were resolved by SDS–7.5% PAGE, transferred onto nitrocellulose membrane, and probed with anti-phospho-Src (PY418) antibodies for 3 h. (Top) Lanes: 1, uninduced HFF cells; 2, HFF cells induced with gBΔTM; 3, uninduced Du3 cells; 4, Du3 cells induced with gBΔTM; 5, uninduced Du17 cells; 6, Du17 cells induced with gBΔTM. Each blot is representative of at least three independent experiments. Src phosphorylation was quantitated as described in the legend to Fig. 1A and expressed as increased fold phosphorylation of Src over that in uninduced cells (assigned a value of 1). (Bottom) After the above reactions, membranes were stripped and reprobed with anti-total-Src antibodies.

about four- and threefold over uninduced cells, respectively (Fig. 4A). Treatment of cells with gBΔTM (1 μg/ml) for 5, 15, and 30 min increased the Src kinase activity 2.5-, 4.4-, and 3.5-fold, respectively (Fig. 4A). Src kinase activity induced by gB was drastically reduced by preincubation of cells with nontoxic doses of the protein tyrosine kinase inhibitors tyrphostin and genistein or with the Src kinase-specific inhibitors PP2 and SU6656 (10), thus demonstrating the specificity of Src activation (Fig. 4A). PI-3K is one of the important downstream effector molecules of FAK and Src activation (15, 17, 22). Phosphorylation of Src by gBΔTM was not affected when cells were incubated with nontoxic doses of the PI-3K inhibitors LY294002 and wortmannin (Fig. 4A). This suggested that Src is an upstream mediator of PI-3K and further demonstrated the specificity of Src phosphorylation.

HHV-8 gBΔTM induction of Src depends on FAK. To determine the role of FAK in the observed gB-induced Src activation, FAK-null primary mouse embryonic fibroblasts (Du3) and FAK-wt Du17 cells were used. Compared to uninduced cells, treatment of HFF cells with gBΔTM activated Src fourfold (Fig. 4B, top, lanes 1 and 2). gBΔTM did not induce Src activity in the FAK-null Du3 cells above the basal level (Fig. 4B, top, lanes 4 and 3); in contrast, there was twofold increase in Src activity in the FAK-wt Du17 cells (Fig. 4B, top, lanes 5 and 6). The total levels of Src in these cells were unchanged (Fig. 4B, bottom), thus demonstrating that gBΔTM was activating pre-existing Src. Taken together, these observations demonstrated that FAK activation is an essential element in the activation of Src by gBΔTM.

HHV-8 gBΔTM induces PI-3K phosphorylation. PI-3Ks are a cellular family of heterodimeric enzymes consisting of a p85 regulatory subunit and p110 catalytic subunit. Phosphorylation of specific tyrosine residues on the p85 subunit is an indication of PI-3K activation as it recruits substrates to the dimer, where they are phosphorylated by the p110 catalytic subunit (15, 40). The products of PI-3K activation, phosphatidylinositol-3,4-bisphosphate and phosphatidylinositol-3,4,5-triphosphate, are increased in activated cells but not in quiescent cells and act as second messengers for a number of cell functions.

Since HHV-8 interaction with target cells induced PI-3K during the early stages of infection (33), we next examined the role of gB in p85 phosphorylation. Serum-starved HFF cells were stimulated with various concentrations of soluble proteins (gBΔTM, gBΔTM-RGA, and ΔTMgpK8.1A) for 30 min alone or in the presence of inhibitors, and the p85 phosphorylation of PI-3K was tested by immunoprecipitation with anti-phosphotyrosine MAb PY20, followed by Western blot analysis with anti-PI-3K p85 antibody. Treatment of HFF cells with 200 ng of EGF per ml and 1 μg of HHV-8 gBΔTM per ml increased the p85 phosphorylation over that in uninduced cells about 6- and 4.5-fold, respectively (Fig. 5A, top, lanes 1 to 3, and B). This PI-3K phosphorylation was dependent on the gB RGD motif, since incubation with 1 μg of gBΔTM-RGA per ml did not elicit any PI-3K phosphorylation (Fig. 5A, top, lane 4, and B). Even higher concentrations did not elicit the response (data not shown). Specificity of PI-3K was shown by the absence of p85 phosphorylation induction by ΔTMgpK8.1A (Fig. 5A, top, lane 5, and B) and in the presence of a nontoxic dose of the PI-3K-specific inhibitor LY294002 (Fig. 5A, top, lane 6, and B). When gB was preincubated with rabbit anti-gB IgG antibodies, about 99% of the gB-induced PI-3K was inhibited, and no significant inhibition was seen with preimmune control IgG antibodies (Fig. 5A, top, lanes 7 and 8, and B). These results further confirmed the specificity of gB-induced phosphorylation of the p85 subunit of PI-3K and suggested that HHV-8 gB alone can initiate the activation of PI-3K.

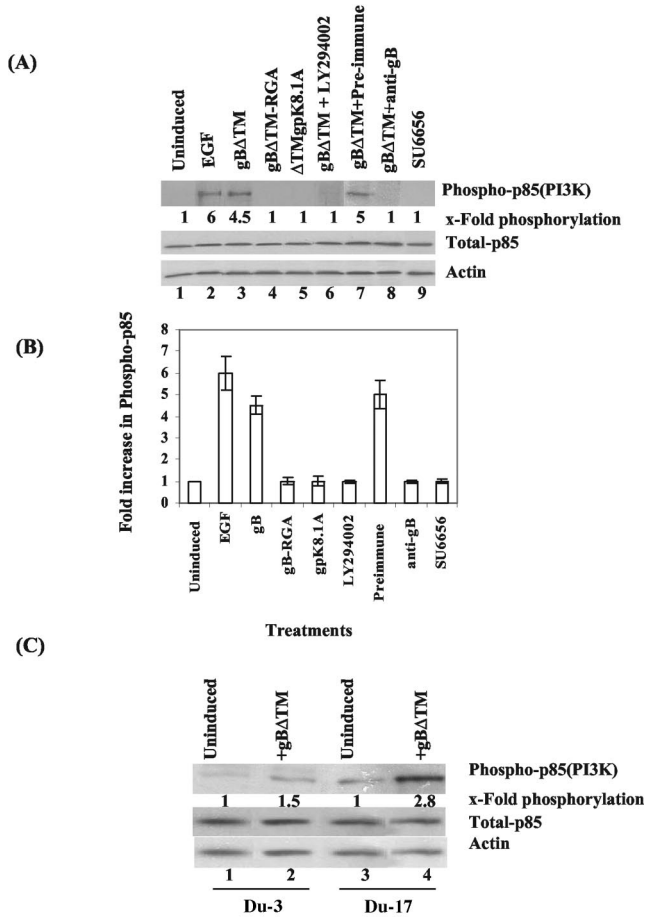

FIG. 5. HHV-8 gBΔTM induces Src-dependent PI-3K phosphorylation. (A) PI-3K activity was assayed in serum-starved HFF cells treated with a variety of ligands and inhibitors. Treated cell lysates were immunoprecipitated for the catalytic complex of PI-3K with anti-phosphotyrosine MAb PY20 for 2 h at 4°C. Immune complexes were Western blotted and probed with anti-PI-3K p85 (Z-8) antibodies. Immunoreactive bands were measured as described in the legend to Fig. 1A. (Top) Lanes: 1, uninduced cells; 2, cells induced with EGF (200 ng/ml) for 15 min; 3, cells induced with gBΔTM (1 μg/ml) for 30 min; 4, cells induced with gBΔTM-RGA (1 μg/ml) for 30 min; 5, cells induced with ΔTMgPK8.1A (1 μg/ml) for 30 min; 6, cells preincubated with LY294002 for 1 h at 37°C before incubation with gBΔTM (1 μg/ml) for 30 min in the presence of inhibitors; 7, cells treated with gBΔTM preincubated with preimmune IgG antibodies; 8, cells treated with gBΔTM preincubated with anti-gB IgG antibodies; 9, cells preincubated with the Src kinase inhibitor SU6656 (2 μM) for 1 h at 37°C before incubation with gBΔTM (1 μg/ml) for 30 min in the presence of inhibitors. PI-3K (p85) phosphorylation in uninduced cells was assigned a value of 1. The total p85 (PI-3K) level was assessed by testing whole-cell lysate in Western blot assays with anti-PI-3K p85α (Z-8) antibodies (middle). Equal loading was confirmed by using actin as a loading control (bottom). Each blot is representative of at least three independent experiments. (B) Immunoreactive bands were quantitated, and band intensity of PI-3K (p85) phosphorylation in uninduced cells was assigned a value of 1 for comparison. Each point represents the average ± the standard deviation of three experiments. (C) PI-3K (p85) phosphorylation induced by 1 μg of gBΔTM per ml at 37°C for 30 min was examined in serum-starved FAK-null Du3 cells and FAK-wt Du17 cells. Lanes: 1, uninduced Du3 cells; 2, Du3 cells induced with gBΔTM; 3, uninduced Du17 cells; 4, Du17 cells induced with gBΔTM. Each blot is representative of at least three independent experiments. Each point represents the average ± the standard deviation of three experiments.

HHV-8 gBΔTM induction of PI-3K depends on Src phosphorylation. PI-3K is an important downstream effector of FAK, which is activated either directly or through Src kinase via Ras (14, 22, 29, 46, 47, 49). Preincubation of cells with nontoxic dose of Src kinase specific inhibitor SU6656 completely blocked the HHV-8 gBΔTM-induced p85 phosphorylation of PI-3K (Fig. 5A, top, lane 9, and B), thus demonstrating that PI-3K is downstream of Src in the gBΔTM-mediated signaling cascade. Treatment of cells with 100 μM genistein also inhibited gB-mediated phosphorylation of the p85 subunit of PI-3K (data not shown). When the levels of total PI-3K activity were assessed by testing whole-cell lysates in Western blot assays with anti-PI-3K p85α (Z-8) antibody (Fig. 5A, middle), no significant change was observed. β-Actin was used as a loading control (Fig. 5A, bottom).

HHV-8 gBΔTM induction of PI-3K depends on FAK phosphorylation. The p85 subunit of PI-3K binds directly to phosphorylated FAK (15, 22, 46, 47, 49). Since interaction of gBΔTM with target cells induced FAK activity, we next examined the role of FAK in PI-3K activation. In FAK-null Du3 cells, no significant PI-3K p85 phosphorylation was stimulated by gBΔTM (Fig. 5C, top, lanes 1 and 2). In contrast, treatment of FAK-wt Du17 cells with gBΔTM stimulated p85 phosphorylation to more than 2.8-fold (Fig. 5C, top, lanes 3 and 4). No change in the total PI-3K and actin levels was observed (Fig. 5C, middle and bottom, respectively). Taken together, these results suggested a critical role for FAK in the induction of PI-3K by gBΔTM. Whether the low level of PI-3K induction (1.5-fold) by gBΔTM in FAK-null Du3 cells was due to the activation of integrin-dependent alternative effectors such as Pyk2 needs to be studied.

HHV-8 gBΔTM induces PI-3K-dependent cytoskeletal rearrangements. Early during infection, HHV-8 induced the polymerization of actin and morphological changes in target cells (33). Among the hallmarks of integrin interaction with ligands are reorganization and remodeling of the actin cytoskeleton, which are controlled by the Rho family of small GTPases, such as RhoA, Rac, and Cdc42 (22, 23, 46, 53). Activated Cdc42 induces the formation of filopodia, thin, finger-like extensions containing actin bundles. Rac regulates the formation of lamellipodia or ruffles, curtain-like extensions often formed along the edge of the cell. Rho mediates the formation of stress fibers, elongated actin bundles that traverse the cells and promote cell attachment to the ECM through Fas (36, 52, 53). Upon FAK and Src phosphorylation, these GTPases can also be activated by PI-3K via intermediate mediators and converge their effects on FA assembly through actin microfilament reorganization and mitogen-activated protein kinase signaling pathways (22, 52). Induction of FAK, Src, and PI-3K by gBΔTM prompted us to examine whether these inductions could induce cytoskeletal reorganization.

HFF cells were serum starved for 24 h, washed, and treated with DMEM or with DMEM containing 1 μg of gBΔTM or gBΔTM-RGA per ml for different periods of time at 37°C. Treated cells were washed, fixed, permeabilized, incubated with rhodamine-labeled phalloidin, and examined under a fluorescence microscope for actin rearrangements. Serum-starved, mock-infected cells exhibited strong peripheral F-actin staining along the cell edges, indicative of cortical actin fibers, and the cell surface margins were well defined and smooth

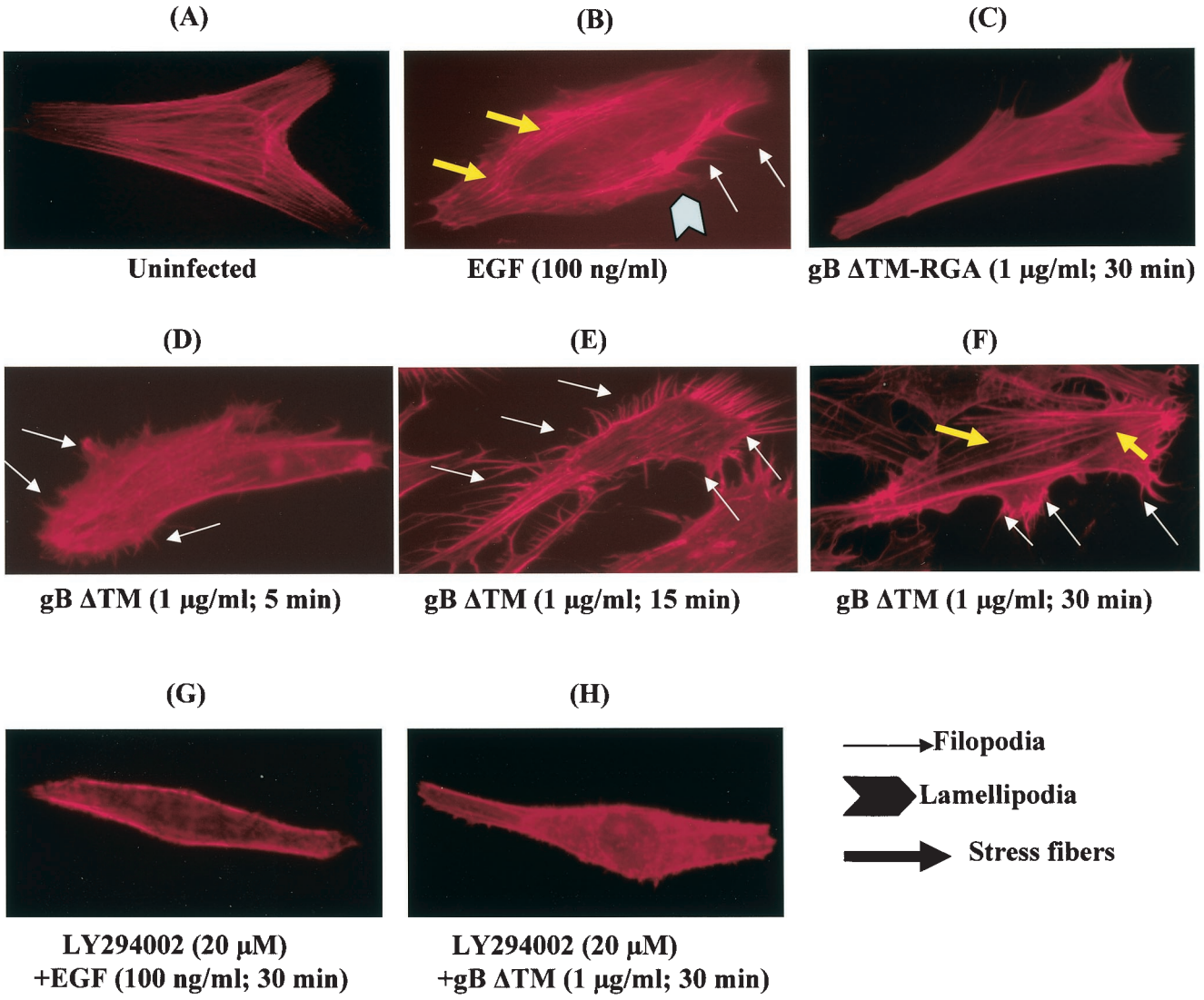

FIG. 6. HHV-8 gBΔTM induces PI-3K-dependent actin cytoskeletal rearrangement. Serum-starved HFF cells incubated with different ligands at 37°C were collected at various time points, fixed, permeabilized, and stained for polymerized actin with rhodamine-labeled phalloidin for 20 min at room temperature. Panels: A, mock-treated cells; B, cells incubated with 100 ng of EGF per ml for 5 min; C, cells incubated with 1 μg of gBΔTM-RGA per ml for 30 min; D, E, and F, cells treated with 1 μg of gBΔTM per ml for 5, 15, and 30 min, respectively; G and H, cells preincubated with the PI-3K inhibitor LY294002 (20 μM) for 1 h at 37°C and induced with EGF (100 ng/ml) and gBΔTM (1 μg/ml) for 30 min, respectively, in the presence of the inhibitor.

(Fig. 6A). Treatment of cells with 1 μg of gBΔTM per ml for 5 and 15 min induced rapid polymerization of actin (Fig. 6D and E, respectively). The increase in F-actin content was associated with the formation of filopodium extensions after as little as 5 min of treatment (Fig. 6D), which became extensive by about 15 min (Fig. 6E). By 30 min, rapid polymerization led into the accumulation of stress fibers within the cells (Fig. 6F). These gB-induced changes were comparable to those in the control EGF-treated cells (Fig. 6B). When cells were incubated with gBΔTM-RGA, no significant changes in the distribution of F-actin were observed, even after 30 min (Fig. 6C), suggesting a role for the interaction between integrins and the RGD motif of gBΔTM in the observed morphological changes. Morphological changes were not observed when cells were preincubated with the PI-3K inhibitor LY294002 before the addition of EGF or gBΔTM (Fig. 6G and H, respectively). Taken together, these findings demonstrated that gBΔTM induced cytoskeletal reorganization in target cells and suggested that PI-3K plays an important role in the observed actin dynamics.

HHV-8 gBΔTM induces Rho GTPases. RhoA, Rac, and Cdc42 Rho GTPases are master regulators of several biological processes via a variety of signaling pathways, including the activation of cytoskeleton rearrangement and morphological changes (22, 37, 38, 39, 53). They cycle between a biologically inactive cytosolic GDP-bound state and an active membrane-bound GTP-bound state. The rate of cycling between the two states is regulated by GTPase-activating proteins that stimulate intrinsic GTPase activity and by guanine nucleotide exchange factors (also designated GDP-GTP exchange factors) that in-

duce the release of GDP, thus enabling GTP binding (22, 23, 37, 38, 39, 53). Since gBΔTM induced morphological changes, to determine the activation of Rho GTPases, gB-induced and uninduced cells fractionated into membrane and cytosolic fractions were analyzed for the membrane translocation of RhoA, Rac, and Cdc42 in Western blot reactions with anti-RhoA, -Rac, and -Cdc42 antibodies. The specificity of this partitioning into membrane and cytosolic fractions and equal loading was confirmed by immunoblotting with antibodies against EGFR as a marker for a protein that specifically partitions to the membrane fraction and antibodies against tubulin as a marker that specifically partitions to the cytosolic fraction (Fig. 7A and B, parts four, lanes 1 to 6). The band intensities were scanned, and for comparison, the activity of the membrane and cytosolic fractions at 0 min (uninduced cells) was taken as onefold.

Relatively low levels of membrane-associated RhoA were detected in cells induced with gBΔTM for 5 and 15 min (Fig. 7A, part one, lanes 2 and 3, and C), which were comparable to those of uninduced HFF cells (Fig. 7A, part 1 [counting from the top], lane 1). However, treatment with gBΔTM for 30 and 60 min resulted in 5.8- and 4.9-fold increases in membrane-associated RhoA (Fig. 7A, part 1, lanes 4 and 5, and C). Coinciding with the RhoA membrane translocation, the levels of cytosolic fractions associated with RhoA were at a maximum at 0 min and decreased over time after incubation with gBΔTM (Fig. 7B, part 1, lanes 1 to 5, and D). When gBΔTM was incubated for 30 min with cells preincubated with the Rho GTPase inhibitor C3 exotoxin for 12 h, no membrane association of RhoA was observed (Fig. 7A, part 1, lane 6, and C), and no decrease in the cytosolic RhoA was observed (Fig. 7B, part 1, lane 6, and C). These results demonstrated the specificity of RhoA activation. The specificity of these findings was also confirmed by the detection of equal levels of the membrane marker EGFR and the cytosolic marker tubulin (Fig. 7A and B, parts 4, lanes 1 to 6).

Under our conditions, we could not observe any membrane-associated Rac in gBΔTM-treated cells (Fig. 7A, part 2, lanes 1 to 6, and C), and the levels of cytosolic fractions associated with Rac were maintained at a constant level (Fig. 7B, part 2, lanes 1 to 6, and D).

Uninduced HFF cells had relatively low levels of membrane-associated Cdc42 (Fig. 7A, part 3, lane 1, and C). After gBΔTM induction, rapid Cdc42 membrane translocation occurred as early as 5 min, was maintained until 15 min, and decreased slowly thereafter (Fig. 7A, part 3, lanes 1 to 5, and C). In contrast, the cytosol-associated Cdc42 level was at a maximum at 0 min and decreased as the time of incubation with gBΔTM increased (Fig. 7B, part 3, lanes 1 to 5, and D). The specificities of these observations were demonstrated by the absence of Cdc42 membrane translocation (Fig. 7A, part 3, lane 6, and C) and no decrease in the cytosolic level of Cdc42 (Fig. 7B, part 3, lane 6, and D) in the C3 exotoxin-treated cells. Taken together, these results demonstrated that gBΔTM activates Cdc42 as early as 5 min and this was maintained even after 60 min, followed by the activation of Rho.

HHV-8 gBΔTM induces Rho GTPase-dependent activation of ezrin. Activated Rho GTPases bind and activate several downstream effector protein kinase molecules such as the members of the myotonic dystrophy-related Cdc42-binding kinase, p^{21}-Cdc42/Rac-activated kinase, and Rho-associated

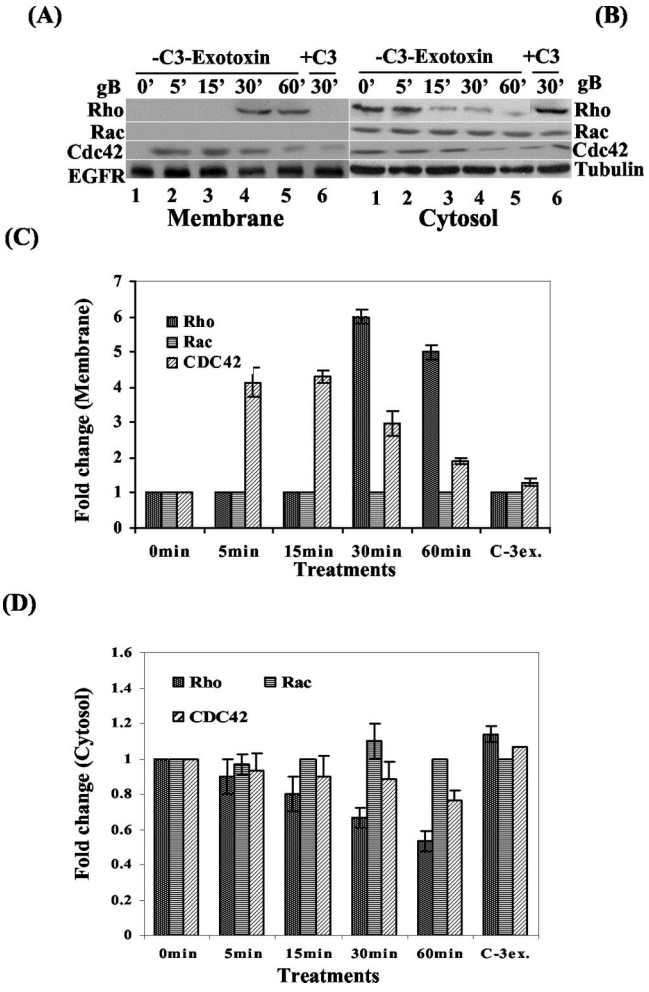

FIG. 7. HHV-8 gBΔTM induces Rho GTPases. Serum-starved HFF cells were treated with 1 μg of gBΔTM per ml for 0, 5, 15, 30, and 60 min. Membrane (A) and cytosolic (B) fractions were prepared with the CNM compartment protein extraction kit, separated by SDS–12.5% PAGE, and immunoblotted with polyclonal rabbit anti-RhoA, -Rac, or -Cdc42 antibodies (first, second, and third parts [counting from the top], respectively, lanes 1 to 5). Lane 6 of panels A and B: HFF cells incubated with 30 μg of C3 exotoxin per ml for 12 h and then induced with gBΔTM for 30 min. Bottom of panels A and B: equal loading of membrane and cytosolic contents measured by immunoblotting with anti-EGFR and anti-tubulin antibodies, respectively. Each blot is representative of at least three independent experiments. (C) Quantitation of gBΔTM-induced RhoA, Rac, and Cdc42 translocation to the membrane. (D) Quantitation of gBΔTM-induced cytosolic content of RhoA, Rac, and Cdc42 in HFF cells. The band intensities in panels A and B were scanned and calculated, and the band intensity at 0 min was assigned a value of 1. Each point represents the average ± the standard deviation of three experiments.

serine/theronine kinase families or scaffolding proteins (23, 37, 38, 39, 53). These effector molecules then interact with several proteins that bring about effects on the actin cytoskeleton and cellular morphology. Since the results presented above demonstrated the ability of gBΔTM to induce morphological changes in target cells via induction of the FAK–Src–PI-3K–Rho GTPase signaling pathway, we next examined the activation of ezrin as an example of the downstream effector molecules. Ezrin belongs to the family of proteins known as the

ERM (ezrin, radixin, and moesin) family of proteins, of which ezrin is the best-studied member. It functions as a cross-linker between the actin cytoskeleton and the plasma membrane and plays structural and regulatory roles in the assembly and stabilization of specialized plasma membrane domains (12, 31, 42). Ezrin has been recently identified as the first cytoskeletal substrate for Lck tyrosine kinase, an early effector of T-cell activation (7). These proteins are found in actin-rich cell surface structures such as filopodia, membrane ruffles, and microvilli, and Rho-dependent formation of these structures requires ERM proteins (31, 38). ERM proteins are also necessary for cell-cell and cell-substrate adhesions, and these proteins interact with several transmembrane adhesion molecules, such as CD44, CD43, and ICAM-1, -2, and -3, and with phosphatidylinositol(4,5)-bisphosphate at the plasma membranes (12, 31, 42). Most of the F-actin binding sites on ERM proteins are in an inactive conformation in the cytoplasm, and their cytoplasm-to-membrane translocation is under the control of Rho GTPase-mediated tyrosine phosphorylation. Ezrin is phosphorylated at two tyrosine residues at amino acids 145 and 353 (12, 31, 42).

To determine the induction of ezrin activity by the gBΔTM-induced Rho GTPase, HFF cells were serum starved and treated with 1 μg of gBΔTM and gBΔTM-RGA per ml for different times, and cell lysates were analyzed in Western blot assays with anti-phospho-ezrin antibodies. Treatment with gBΔTM for 5 and 15 min resulted in 3- and 2.5-fold increases in ezrin activity over that of uninduced cells, but the activity returned to normal levels by 30 min (Fig. 8A, top, lanes 1 to 4). When cells were incubated with a nontoxic dose of the Rho GTPase inhibitor C3 exotoxin for 12 h before incubation with gBΔTM, activation of ezrin was completely inhibited (Fig. 8A, top, lane 5). Ezrin phosphorylation was not detected in cells treated with gBΔTM-RGA (Fig. 8A, top, lanes 6 and 7), and bFGF, which was used as a positive control, activated ezrin fourfold (Fig. 8A, top, lane 8). Reprobing of the membranes with anti-actin antibodies (Fig. 8A, bottom) suggested the activation of endogenous ezrin. These results demonstrated the specificity of ezrin induction by gBΔTM, which was dependent on Rho GTPase activation. To morphologically confirm the ezrin activation observed, colocalization of ezrin with actin was analyzed with anti-phospho-ezrin antibodies and phalloidin staining. In uninduced HFF cells, the distribution of ezrin is more diffuse (Fig. 8B, bottom). In contrast, in cells induced with gBΔTM for 30 min, ezrin was localized in the periphery of the cells in a distinct patchy pattern (Fig. 8B, top two parts). Image overlays demonstrated the colocalization of ezrin with actin (Fig. 8B). The specificity of this induction was shown by the absence of ezrin activation in the gBΔTM-RGA-treated cells (Fig. 8B, third part). Taken together, these results demonstrated that gBΔTM, via its RGD motif interaction with integrin, induces the host cell FAK–Src–PI-3K–Rho GTPase signaling pathways.

Inhibition of tyrosine kinases by genistein inhibits HHV-8 infection of target cells. We have previously shown the integrin-FAK-dependent activation of the PI-3K–PKCζ–MEK–ERK mitogenic signal pathway early during HHV-8 infection and the reduction of infectivity by PI-3K, PKCζ, MEK, and ERK inhibitors (33). The results presented here suggest that, independently of other viral glycoproteins, HHV-8 gB alone can induce the integrin-dependent preexisting FAK–Src–PI-3K–Rho GTPase cellular tyrosine kinases, thus implying the existence of a critical role for the HHV-8 gB-induced cellular kinases during the virus binding and entry stage of infection. These signal pathways may provide an opportunistic environment for the infection of target cells by modulating the different stages of infection, such as virus internalization, release of capsid into the cytoplasm, transport of virus capsid to the cell nucleus, delivery of viral DNA into the nucleus, and viral latent and/or lytic gene transcription. Since examining the role played by these cellular kinases in HHV-8 infection of FAK-, Src-, PI-3K-, and Rho-GTPase-negative cells and/or cells expressing dominant negative mutants was beyond the scope of these studies, we used genistein, a general inhibitor of tyrosine kinases, including FAK, Src, and PI-3K, to define the physiological role of this signal pathway induced by HHV-8 gB. Cells were incubated with genistein for 1 h before infection with GFP–HHV-8 for 2 h in the presence of the drug. Under these conditions, cell viability and the expression of other proteins were not affected (data not shown). As shown before (2), preincubation of the virus with 100 μg of heparin inhibited HHV-8 infection by ~85%. Genistein blocked viral infectivity in a dose-dependent manner (Fig. 9A), with an ~90% reduction of GFP–HHV-8 infectivity at nontoxic concentrations of 100 and 200 μM (Fig. 9A). Since these concentrations have been shown to reduce HHV-8- and HHV-8 gB-induced FAK (59) without affecting the binding of radiolabeled HHV-8 to HFF cells (data not shown), these results suggested that genistein affected the post-HS binding stage of infection, thus demonstrating that activation of tyrosine kinases is essential for HHV-8 entry and infection of target cells.

Genistein affects the internalization of HHV-8 in target cells. In the GFP–HHV-8 infectivity assay used above, the readings were taken after 3 days p.i. Since genistein could block HHV-8 infection by interference at different stages of infection, to further determine the significance of the neutralization of GFP–HHV-8, we examined its effect on HHV-8 internalization. To estimate the internalized virus load, we have previously carried out a DNA PCR assay with primers amplifying the HHV-8 ORF25 gene (33). Since this method suffered from low sensitivity toward saturation of the amplification curve and manual errors in the estimation of intensity of the amplified products on a gel, we carried out a quantitative real-time DNA PCR assay (32). With this method, we have previously shown that internalized viral DNA could be detected in HFF cells as early as 5 min p.i., increasing rapidly during the first 60 to 90 min of infection and reaching a plateau at around 90 to 120 min p.i. Preincubation of the virus with 100 μg of heparin per ml blocked HHV-8 DNA entry by more than 90% (Fig. 9B). Treatment of HFF cells with the mitogen-activated protein kinase (MEK) inhibitor U0126 did not show any significant reduction of HHV-8 DNA internalization (Fig. 9B). In contrast, a dose-dependent reduction of HHV-8 DNA internalization was observed with genistein, with an ~90% reduction of internalization at a 100 μM concentration (Fig. 9B). Preincubation with the PI-3K inhibitor LY294002 at 50 and 100 μM also reduced the internalization by about 65 to 78% (Fig. 9B). These studies suggested that the inhibition of GFP–HHV-8 infectivity by genistein and the PI-3K inhibitors (33) is probably due to a block at the entry stage of HHV-8

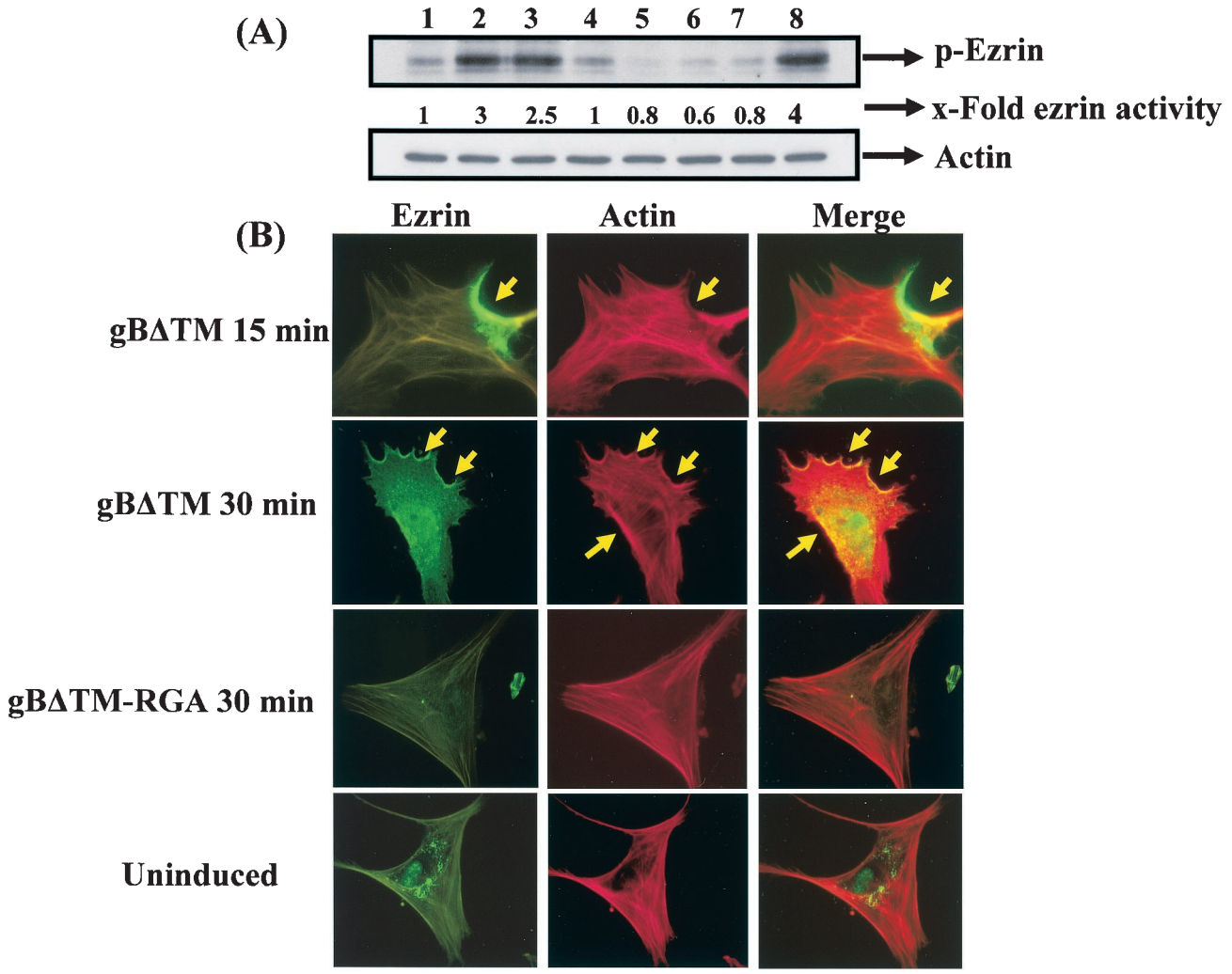

FIG. 8. HHV-8 gBΔTM induces ezrin phosphorylation. (A) Ezrin phosphorylation was detected in serum-starved HFF cell lysates by immunoblotting with anti-phospho-ezrin antibodies. Lysates were normalized to contain ~10 μg of total protein. Immunoreactive bands were visualized with HRP-conjugated secondary antibodies and the enhanced-chemiluminescent system. (Top) Lanes: 1, cells incubated with PBS; 2 to 4, cells incubated with 1 μg of gBΔTM per ml for 5, 15, and 30 min, respectively; 5, cells incubated with 30 μg of C3 exotoxin per ml for 12 h before incubation with 1 μg of gBΔTM per ml for 30 min in the presence of inhibitor; 6 and 7, cells incubated with 1 μg of gBΔTM-RGA per ml for 5 and 15 min, respectively; 8, cells incubated with 50 ng of bFGF per ml for 5 min. Each blot is representative of at least three independent experiments. The band intensities were scanned and calculated, and uninduced-cell intensity was assigned a value of 1. (B) Colocalization of ezrin with F-actin in gBΔTM-induced cells. Serum-starved HFF cells grown in eight-well chamber slides were treated with 200 μl of PBS or 1 μg of gBΔTM or gBΔTM-RGA per ml for 15 min at 37°C. After incubation, cells were washed, fixed, permeabilized, reacted with anti-phospho-ezrin antibodies for 30 min at room temperature, and reacted with FITC-conjugated secondary antibodies for 30 min at room temperature, followed by rhodamine-labeled phalloidin for 20 min at room temperature. The arrows indicate representative areas of phosphorylated ezrin-actin colocalization.

infection, thus suggesting that the activation of tyrosine kinases, including PI-3K, plays a role in HHV-8 entry into target cells. Inhibition of HHV-8 infectivity by the inhibitors of MEK (33) without affecting viral entry suggests a role for activation of the MEK pathway (33) at a post-viral-entry stage of infection.

To ascertain the specificity of these observations further, HHV-8 gene expression was examined by quantitative real-time RT-PCR. Infection of in vitro target cells by HHV-8 is characterized by the expression of the latency-associated ORF73 gene (LANA-1) and the absence of progeny virus production. We have shown recently that early during infection, in addition to the latency-associated genes, HHV-8 also expresses a limited number of lytic-cycle genes, including the lytic-cycle switch gene ORF50 (RTA) (25). Preincubation of the virus with 100 μg of heparin per ml blocked more than 80% of HHV-8 ORF73 and ORF50 gene expression (Fig. 9C). A dose-dependent reduction in ORF73 and ORF50 gene expression was observed with genistein, with an ~80% reduction at a 100 μM concentration (Fig. 9C). Similarly, treatment of cells with the PI-3K inhibitor LY294002 decreased ORF73 and ORF50 gene expression in a dose-dependent manner (Fig. 9C). In contrast, cellular GAPDH gene expression, which was used to normalize the viral RNA copy numbers, was not af-

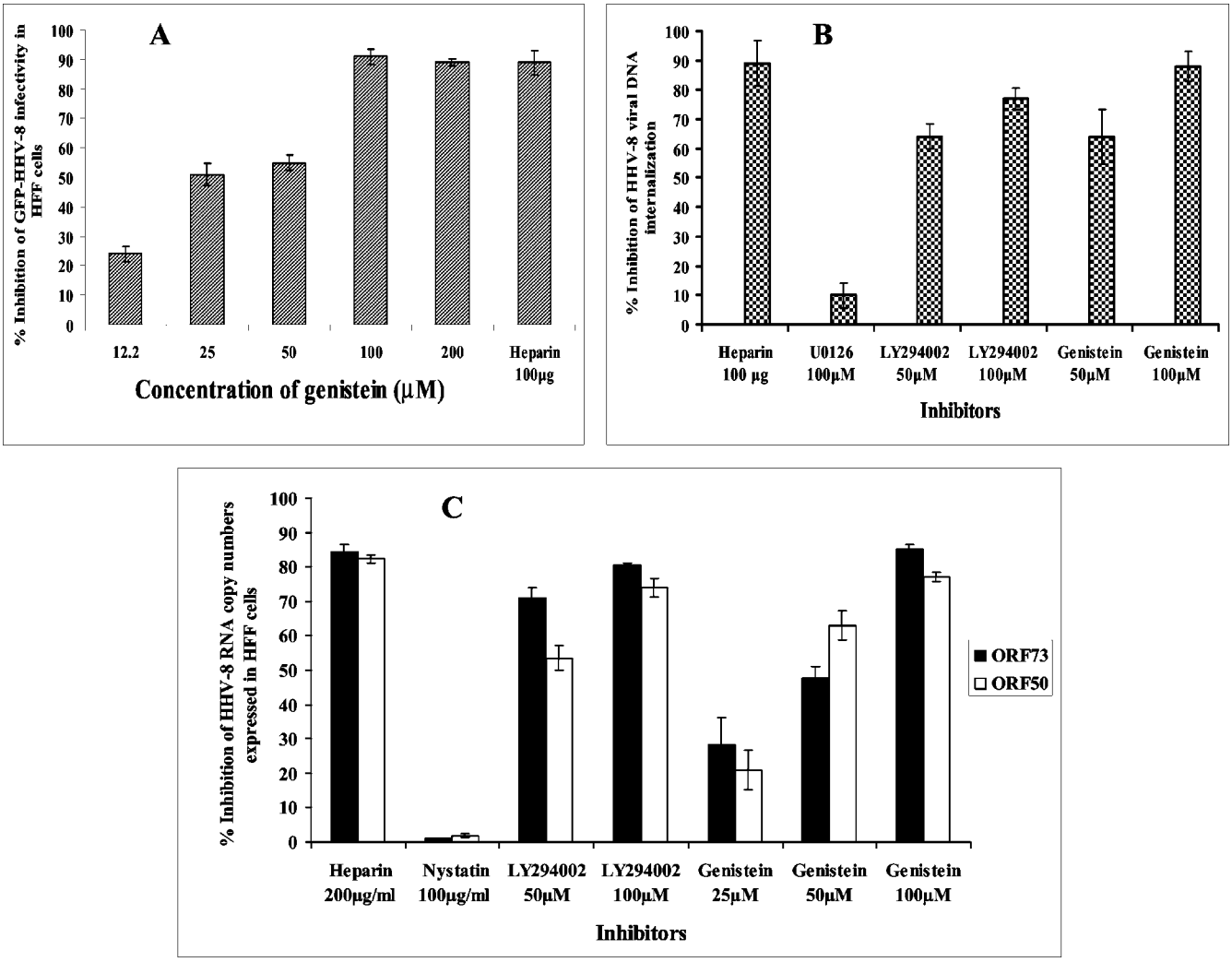

FIG. 9. Inhibition of cellular tyrosine kinases blocks HHV-8 entry and infection. (A) HFF cell monolayers incubated with DMEM or with DMEM containing various concentrations of genistein for 1 h at 37°C were infected with GFP–HHV-8 in the presence or absence of genistein at 37°C for 2 h, washed twice with DMEM, and further incubated with growth medium at 37°C. For a control, virus was preincubated with 100 μg of heparin per ml for 1 h at 37°C before addition to cells. After 3 days, infection was monitored by counting green fluorescent cells. Data are presented as a percentage of the inhibition of virus infectivity obtained when cells were incubated with the virus alone. Each reaction was done in triplicate, and each point represents the average ± the standard deviation of three experiments. (B) HFF cells or HFF cells incubated with different concentrations of protein tyrosine kinase inhibitors for 1 h at 37°C and infected with HHV-8 at 10 DNA copies/cell. For a control, the virus was preincubated with 100 μg of heparin per ml for 1 h at 37°C before addition to cells. After 2 h of incubation, cells were washed twice with PBS to remove the unbound virus, treated with trypsin-EDTA for 5 min at 37°C to remove the bound but noninternalized virus, and washed, and then total DNA was isolated. This was normalized, and HHV-8 ORF73 copy numbers were estimated by real-time DNA PCR. The Ct values were used to plot the standard graph and to calculate the relative copy numbers of viral DNA in the samples. Data are presented as a percentage of the inhibition of HHV-8 DNA internalization obtained when cells were incubated with the virus alone. Each reaction was done in duplicate, and each point represents the average ± the standard deviation of three experiments. (C) Untreated HFF cells or HFF cells incubated with inhibitors for 1 h at 37°C were infected with HHV-8 at 10 DNA copies/cell and incubated for 2 h, total RNA was isolated and treated with DNase I, and HHV-8 ORF50 and ORF73 transcripts were detected by real-time RT-PCR with gene-specific TaqMan probes. Known concentrations of gene-specific transcripts from the cloned genes were used as external control samples. All samples were used in separate real-time DNA PCRs (without RT) to confirm the absence of contaminating DNA. The relative copy numbers of the transcripts were calculated and normalized with the values of GAPDH control reactions. Data are presented as a percentage of the inhibition of the HHV-8 RNA copy numbers obtained when cells were incubated with the virus alone. Each reaction was done in duplicate, and each point represents the average ± the standard deviation of three experiments.

fected, suggesting that the PI-3K inhibitors did not affect general transcription. We have previously shown that treatment of cells with nystatin, an inhibitor of the caveola-dependent pathway, did not significantly alter HHV-8 infection of HFF cells (2). Similar to this observation, in the present study, nystatin did not have any effect on ORF73 and ORF50 gene expression (Fig. 9C). These studies suggested that genistein and PI-3K inhibitors block the entry stage of HHV-8 infection and thus suggest that the activation of cellular tyrosine kinases by HHV-8 gB plays roles in virus entry into target cells.

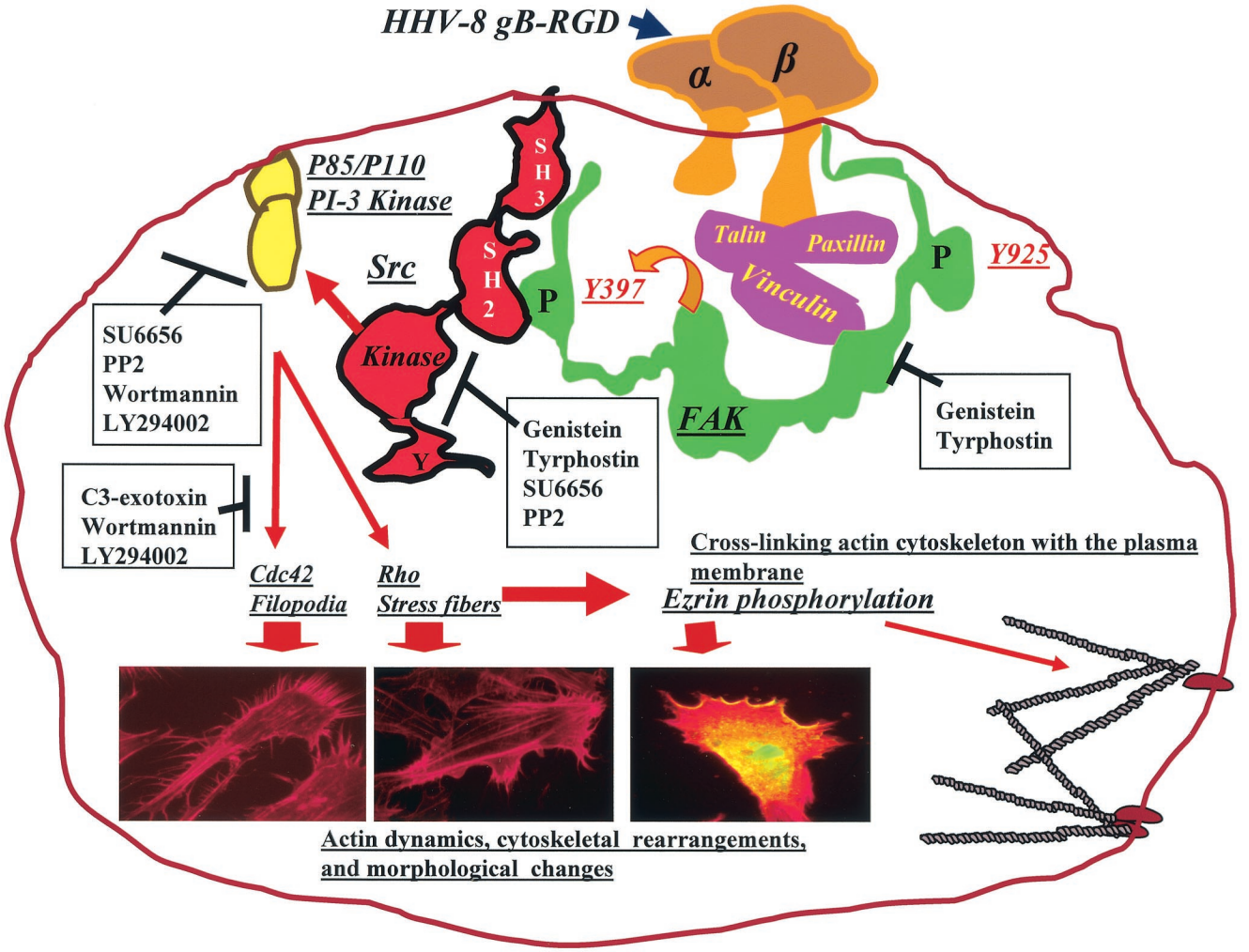

FIG. 10. FAK–Src–PI-3K–Rho GTPase signaling pathways induced by HHV-8 gB. A diagrammatic representation of the gB-integrin-induced cascade of signaling pathways deciphered in this study is shown. Following HHV-8 gB interactions with cell surface integrins, FAK is autophosphorylated at Tyr^{397}, which creates a binding site for the SH2 domain of Src family kinases and subsequent tyrosine phosphorylation. Activated Src phosphorylates p85 of PI-3K, which in turn activates the RhoA and Cdc42 Rho GTPases, resulting in changes in actin dynamics, cytoskeletal rearrangement, and morphological changes. Inhibitors of FAK, Src, PI-3K, and Rho GTPases are boxed, and the stages of interference are shown by the solid lines. Morphological changes induced by gB in HFF cells are shown, and the thick arrows indicate the inducing Rho GTPase protein and ezrin.

DISCUSSION

Eukaryotic cells interact with their extracellular environment via numerous cell surface molecules. The ensuing multitudes of biological processes are mediated by a highly interlinked network of signal pathways (11, 46, 47, 49, 55, 57). Ligand mimicry is an opportunistic mechanism by which microbes subvert host signaling molecules for their benefit (11, 55, 57). Among the several glycoproteins predicted to be encoded by HHV-8 (35, 45), previous studies have demonstrated the molecular identity of gB, gpK8.1A, gH, and gL; their association with virion envelopes; and their potential role in virus infectivity (4, 5, 34, 59, 62). Even though gB is highly conserved among herpesviruses, only HHV-8 gB possesses the RGD motif, interacts with α3β1 integrin molecules, and uses it as a cellular receptor for entry into target cells (5). In the present study, summarized in Fig. 10, we show that by its interaction with integrin, HHV-8 gB induces the integrin-dependent preexisting FAK–Src–PI-3K–Rho GTPase signaling pathways. Together with our demonstration of integrin-dependent FAK–PI-3K signal pathway induction and morphological changes caused by HHV-8 (33), these results suggest that soluble gB mimics some of the signaling pathways induced by HHV-8 during the early stages of target cell infection.

The similarity of the full-length gB and gBΔTM proteins in terms of processing and heterodimer formation (4, 8, 58), maintenance in a soluble form, and activation of FAK in target cells suggests that gBΔTM possesses a conformation similar to that of the external domain of gB. The absence of LPS contamination in our protein preparations, the inhibition of signal pathway induction by anti-gB antibodies, and the requirement of the gB RGD motif for activation clearly demonstrated the specificity of gBΔTM-induced signaling pathways. Even though

gBΔTM-RGA also binds to target cells as efficiently as does gBΔTM via its interaction with cell surface HS (4, 59), the absence of signal induction by gBΔTM-RGA suggests a role for integrin, but not HS, molecules in the signal pathway deciphered in this study.

FAK activation is one of the key steps that follow immediately after integrin-ligand interaction (5). The demonstration of FAK activation by HHV-8 is the first in a herpesvirus. The ability of soluble human α3β1 integrin to block FAK induction by HHV-8 gB and studies with CHO cells clearly indicate that FAK signaling induced by HHV-8 gB is at least in part mediated via α3β1 integrin. Moreover, studies with FAK-null mouse Du3 cells further confirmed that the α3β1 integrin and FAK play roles in gB-mediated signal induction. We have previously shown that [^{3}H]thymidine-labeled HHV-8 bound both FAK-wt Du17 and FAK-null Du3 cells with the same efficiency and that this binding was inhibited by soluble heparin (33). However, HHV-8 infectivity was reduced by more than 90% in Du3 cells (33), which demonstrated that the reduced infectivity in Du3 cells could be due to a block in the entry into these cells or a block in the delivery of viral DNA into the nucleus. These results, together with the activation of FAK by soluble gB and the inhibition of FAK activation and HHV-8 entry by genistein, suggest a key role for FAK in HHV-8 infection. Further work is in progress to decipher the interlinkage among FAK activation, virus entry, and infection.

Although integrin α3β1 lacks an intracellular catalytic domain, its association with a cytoplasmic tyrosine kinase is responsible for initiating the outside-in signaling pathways (46, 47, 48, 49). Existing models of FAK and Src activation in integrin signaling have placed the activation of FAK upstream of Src (22, 46, 47, 48). FAK acts as a scaffolding molecule, phosphorylated FAK-Y^{397} serves as the binding site for the SH2 domain of Src, and this FAK-Src interaction is stabilized by the SH3 domain of Src (54). Once this complex is formed, the inhibitory Src-SH2-pY^{527} intramolecular interaction is disrupted, thus increasing the Src catalytic activity (22, 46, 47, 48, 49). The inability of gBΔTM to activate Src in FAK-null Du3 cells and in genistein- and tyrphostin-treated cells clearly demonstrates that in the gBΔTM-mediated signal transduction events, FAK is upstream of Src activation. Activated Src kinases phosphorylate two cytoskeletal proteins, paxillin and tensin, which localize at the FA sites (22, 46, 47, 48, 49). When coupled with our previous demonstration of colocalization of paxillin with FAK in gBΔTM-induced target cells (58), these results suggest that gB-FAK-Src activation leads to further activation of cytoskeleton-associated proteins. Since Src is a vital link between integrin and other receptor-mediated signaling with a variety of cellular functions, including endocytosis, the role of Src in HHV-8 entry and infection needs to be examined.

The mechanism by which the herpesvirus envelope glycoprotein-receptor interactions facilitate infection is not well understood. The ability of HHV-8 gB to induce integrin-dependent FAK–Src–PI-3K activation, the substantial reduction of virus entry by inhibition of tyrosine kinases, and the reduction of infectivity in FAK-negative cells suggest that HHV-8 gB-induced signal pathways may play important roles in virus infection of target cells. Integrins play major roles in the infectious process of many microbes, including several viruses that enter cells by endocytosis (11, 55, 57). Nonenveloped viruses like adenoviruses (αVβ3, αVβ5, αVβ1), echovirus (α2β1), foot-and-mouth disease virus (αVβ1, αVβ1, αVβ6), rotaviruses (α2β1, αVβ3), human parechovirus (αVβ3, αVβ1), and papillomaviruses (α6β4, α6β1), as well as the enveloped hantavirus (αVβ3), have been reported to use one or more integrin molecules during the infection process (2, 5, 26, 27, 55). Interestingly, adenovirus, echovirus, foot-and-mouth disease virus, parechovirus, parvovirus, rotavirus, and hantavirus, interacting with integrins, enter target cells via endocytosis (2, 5, 26, 27, 55). This is probably due to the fact that ligand interactions with integrins activating FAK, Src, and other integrin-linked kinases are intimately associated with endocytosis (22, 28, 30, 60). Our recent studies demonstrated that HHV-8 enters HFF cells by endocytosis and that for infectious entry, HHV-8 uses clathrin-mediated endocytosis and a low-pH intracellular environment (2). Engagement of integrin by gB and HHV-8's entry by endocytosis suggest that activation of the FAK-dependent signal pathways by gB may have an important role in infection. Signal pathways are intimately linked with the formation of clathrin and other endocytic vesicles (22, 28, 30, 60). The integrin-FAK-dependent activation of Src by HHV-8 gB may have an important role in the endocytosis of virus particles, since recent studies have shown that Src-mediated tyrosine phosphorylation of clathrin regulates clathrin translocation to the plasma membrane (60). Entry of HHV-8 by endocytosis; activation of Src by HHV-8 gB, a critical element required for the formation and regulation of clathrin and dynamin; and the inhibition of virus entry by genistein suggest that gB-integrin-induced signal pathways may facilitate virus uptake into cells. Further work is in progress to define the roles of FAK and Src in the activation of clathrin and dynamin and in the formation of endocytic vesicles and endocytosis of HHV-8.

Induction of PI-3K by gB in an integrin-FAK-Src-dependent manner, together with our observation that blocking of PI-3K activity interferes in HHV-8's entry (33), suggests critical roles for the gB-induced FAK–Src–PI-3K pathway in infection. FAK activation and cytoskeleton assembly have been shown to be essential for the endocytosis of several microbes (14, 18, 19, 55). For example, adenovirus entry into target cells via endocytosis depends on actin cytoskeleton activation by the Rho family of GTPases, and PI-3K has been proposed to modulate adenovirus entry (22, 29, 30). Uptake of influenza virus into polarized epithelial cells requires actin cytoskeleton reorganization mediated by Rac (55). Similarly, PI-3K-dependent HHV-8 gB activation of Rho-GTPases and ezrin and the subsequent modulation of actin may also have a profound effect on virus entry and infection, since activated Rac, Rho, Cdc42, and Rab5 act as molecular switches in various signal transduction pathways and are essential for the modulation of actin dynamics, the formation of endocytic vesicles and their fission, cytoskeletal transport, endosome movement, fusion of endocytic vesicles, and recycling (14, 18, 22, 23, 28, 30). Actin provides the mechanical force required for endosome formation and propulsion of endocytic vesicles and acts as a structural platform stabilizing the half-life of signaling molecules in the cell, including integrins (14, 44, 53). Actin cytoskeleton reorganization plays an important role in viral entry, as cytoskeletal elements such as microtubules and microfilaments

have long been recognized as crucial in controlling the intracellular movement of viruses (18, 26, 27, 55). Cdc42 can be directly linked to the microtubule network via its target, CIP4, which interacts with both WASP and microtubules (22, 44, 49, 58). Rho's activation of diaphan and Rac's activation of Pak/stathmin are required for microtubular stabilization (22, 44, 49, 58), all of which regulate the movement of endocytic vesicles, and probably for the movement of the capsid-tegument of HHV-8 that is released into the cytoplasm. Studies are in progress to examine the signaling and role of microtubules in HHV-8 infection.

In summary, interaction of HHV-8 gB with integrins (5, 58), entry of HHV-8 by endocytosis into HFF and BJAB cells (3, 7), the ability of gB to induce integrin-dependent pre-existing FAK–Src–PI-3K–Rho GTPase signal pathways that play vital roles in host cell endocytosis and movement of particulate materials in the cytoplasm, and the ability of tyrosine kinase inhibition to block virus entry suggest that HHV-8 gB-integrin interaction-induced signal pathways may provide a very conducive environment for the successful infection of target cells. Further studies with FAK-, Src-, and PI-3K-negative cells and cells expressing dominant negative mutant proteins are essential to decipher the interlinks between these cellular kinases and the stages of virus infection, which would aid in the development of novel strategies to control HHV-8 infection.

ACKNOWLEDGMENTS

This study was supported in part by Public Health Service grants CA 75911 and 82056 to B.C. and by a University of Kansas Medical Center Biomedical research training program postdoctoral fellowship to P.P.N.

We thank Shaw M. Akula for morphological analyses and Marilyn Smith for critically reading the manuscript.

REFERENCES

1. **Akiyama, T., J. Ishida, S. Nakagawa, H. Ogawara, S. Watanabe, N. Itoh, M. Shibuya, and Y. Fukami.** 1987. Genistein, a specific inhibitor of tyrosine-specific protein kinases. J. Biol. Chem. **262:**5592–5595.
2. **Akula, S. M., N. P. Pramod, N. S. Walia, F. Z. Wang, B. Fegley, and B. Chandran.** 2003. Kaposi's sarcoma-associated herpesvirus (human herpesvirus 8) infection of human fibroblast cells occur through endocytosis. J. Virol. **77:**7978–7990.
3. **Akula, S. M., F. Z. Wang, J. Vieira, and B. Chandran.** 2001. Human herpesvirus 8 (HHV-8/KSHV) infection of target cells involves interaction with heparan sulfate. Virology **282:**245–255.
4. **Akula, S. M., N. P. Pramod, F. Z. Wang, and B. Chandran.** 2001. Human herpesvirus envelope-associated glycoprotein B interacts with heparan sulfate-like moieties. Virology **284:**235–249.
5. **Akula, S. M., N. P. Pramod, F. Z. Wang, and B. Chandran.** 2002. Integrin $\alpha 3\beta 1$ (CD 49c/29) is a cellular receptor for Kaposi's sarcoma-associated herpesvirus (KSHV/HHV-8) entry into the target cells. Cell **108:**407–419.
6. **Antman, K., and Y. Chang.** 2000. Kaposi's sarcoma. N. Engl. J. Med. **342:**1027–1038.
7. **Autero, M., L. Heiska, L. Ronnstrand, A. Vaheri, C. G. Gahmberg, and O. Carpen.** 2003. Ezrin is a substrate for Lck in T cells. FEBS Lett. **535:**82–86.
8. **Baghian, A., M. Luftig, J. B. Black, Y. Meng, C. Pau, T. Voss, P. E. Pellett, and K. G. Kousoulas.** 2000. Glycoprotein B of human herpesvirus 8 is a component of the virion in a cleaved form composed of amino-and carboxy-terminal fragments. Virology **269:**18–25.
9. **Birkmann, A., A. Mahr, A. Ensser, S. Yaguboglu, F. Titgemeyer, B. Fleckenstein, and F. Neipel.** 2001. Cell surface heparan sulfate is a receptor for human herpesvirus 8 and interacts with envelope glycoprotein K8.1. J. Virol. **75:**11583–11593.
10. **Blake, R. A., M. A. Broome, X. Liu, J. Wu, M. Gishizky, L. Sun, and S. A. Coutneidge.** 2000. SU6656, a selective Src family kinase inhibitor, used to probe growth factor signaling. Mol. Cell. Biol. **20:**9018–9027.
11. **Bliska, J. B., J. E. Galan, and S. Falkow.** 1993. Signal transduction in the mammalian cell during bacterial attachment and entry. Cell **73:**903–920.
12. **Bretscher, A., D. Reczek, and M. Berryman.** 1997. Ezrin: a protein requiring conformational activation to link microfilaments to the plasma membrane in the assembly of cell surface structures. J. Cell Sci. **110:**3011–3018.
13. **Calalb, M. B., T. R. Polte, and S. K. Hanks.** 1995. Tyrosine phosphorylation of focal adhesion kinase at sites in the catalytic domain regulates kinase activity: a role for Src family kinases. Mol. Cell. Biol. **15:**954–963.
14. **Calderwood, D. A., S. J. Shattil, and M. H. Ginsberg.** 2000. Integrins and actin filaments: reciprocal regulations of cell adhesions and signaling. J. Biol. Chem. **275:**22607–22610.
15. **Cantley, L. C.** 2002. The phosphoinositide 3-kinase pathway. Science **296:**1655–1657.
16. **Chang, Y., E. Cesarman, M. S. Pessin, F. Lee, J. Culpepper, D. M. Knowles, and P. S. Moore.** 1994. Identification of herpesvirus-like DNA sequences in AIDS-associated Kaposi's sarcoma. Science **266:**1865–1869.
17. **Clark, E. A., and J. S. Brugge.** 1995. Integrins and signal transduction pathways: the road taken. Science **268:**233–239.
18. **Cudmore, S., I. Reckmann, and M. Way.** 1997. Viral manipulations of the actin cytoskeleton. Trends Microbiol. **5:**142–148.
19. **Dramsi, S., and P. Cossart.** 1998. Intracellular pathogens and the actin cytoskeleton. Annu. Rev. Cell Dev. Biol. **14:**137–166.
20. **Fakhari, F. D., and D. P. Dittmer.** 2002. Charting latency transcripts in Kaposi's sarcoma-associated herpesvirus by whole-genome real-time quantitative PCR. J. Virol. **76:**6213–6223.
21. **Ganem, D.** 1998. Human herpesvirus 8 and its role in the genesis of Kaposi's sarcoma. Curr. Clin. Top. Infect. Dis. **18:**237–251.
22. **Giancotti, F. G., and E. Ruoslahti.** 1999. Integrin signaling. Science **285:**1028–1032.
23. **Hall, A.** 1998. Rho GTPases and the actin cytoskeleton. Science **279:**509–514.
24. **Ilic, D., Y. Furuta, S. Kanazawa, N. Takeda, K. Sobue, N. Nakatsuji, S. Nomura, J. Fujimoto, M. Okada, and T. Yamamoto.** 1995. Reduced cell motility and enhanced focal adhesion contact formation in cells from FAK-deficient mice. Nature **377:**539–544.
25. **Krishnan, H. H., P. P. Naranatt, M. S. Smith, L. Zeng, C. Bloomer, and B. Chandran.** 2004. Concurrent expression of latent and a limited number of lytic genes with immune modulation and antiapoptotic function by Kaposi's sarcoma-associated herpesvirus early during infection of primary endothelial and fibroblast cells and subsequent decline of lytic gene expression. J. Virol. **78:**3601–3620.
26. **Li, E., D. Stupack, G. M. Bokoch, and G. R. Nemerow.** 1998. Adenovirus endocytosis requires actin cytoskeleton reorganization mediated by Rho family GTPases. J. Virol. **72:**8806–8812.
27. **Li, E., D. Stupack, R. Klemke, D. A. Cheresh, and G. R. Nemerow.** 1998. Adenovirus endocytosis via α_v integrins requires phosphoinositide-3-OH Kinase. J. Virol. **72:**2055–2061.
28. **Marsh., M., and H. T. McMahon, and H. T.** 1999. The structural era of endocytosis. Science **285:**215–221.
29. **McLean, G. W., V. J. Fincham, and M. C. Frame.** 2000. V-Src induces tyrosine phosphorylation of focal adhesion kinase independently of tyrosine 397 and formation of a complex with Src. J. Biol. Chem. **275:**23333–23339.
30. **McPherson, P. S., B. K. Kay, and N. K. Hussain.** 2001. Signaling on the endocytic pathway. Traffic **2:**375–384.
31. **Nakamura, N., N. Oshiro, Y. Fukata, M. Amano, M. Fukata, S. Kuroda, Y. Matsuura, T. Leung, L. Lin, and K. Kaibuchi.** 2000. Phosphorylation of ERM proteins at filopodia induced by Cdc42. Genes Cells **5:**571–581.
32. **Naranatt, P. P., H. H. Krishnan, S. R. Svojanovsky, C. Bloomer, S. Mathur, and B. Chandran.** 2004. Host gene induction and transcriptional reprogramming in Kaposi's sarcoma-associated herpesvirus (KSHV/HHV-8) infected endothelial, fibroblast and B cells: insights into modulation events early during infection. Cancer Res. **64:**72–84.
33. **Naranatt, P. P., S. M. Akula, C. A. Zien, H. H. Krishnan, and B. Chandran.** 2003. Kaposi's sarcoma-associated herpesvirus induces the phosphatidylinositol 3-kinase-PKCζ-MEK-ERK signaling pathway in target cells early during infection: implications for infectivity. J. Virol. **77:**1524–1539.
34. **Naranatt, P. P., S. M. Akula, and B. Chandran.** 2002. Characterization of $\gamma 2$-human herpesvirus-8 glycoproteins gH and gL. Arch. Virol. **147:**1349–1370.
35. **Neipel, F., J. C. Albrecht, and B. Fleckenstein.** 1997. Cell-homologous genes in the Kaposi's sarcoma-associated rhadinovirus human herpesvirus 8: determinants of its pathogenicity? J. Virol. **71:**4187–4192.
36. **Nishiyama, T., T. Sasaki, K. Takaishi, M. Kato, H. Yaku, K. Araki, Y. Matsuura, and Y. Takai.** 1994. *rac* p21 is involved in insulin-induced membrane ruffling and *rho* p21 is involved in hepatocyte growth factor- and 12-*O*-tetradecanoylphorbol-13-acetate (TPA)-induced membrane ruffling in KB cells. Mol. Cell. Biol. **14:**2447–2456.
37. **Nowak, F., A. Jacquemin-Sablon, and J. Pierre.** 1997. Epidermal growth factor receptor signaling cascade as target for tyrphostin (RG50864) in epithelial cells. Paradoxical effects of mitogen-activated protein kinase-kinase and mitogen-activated protein kinase activities. Biochem. Pharmacol. **53:**287–298.
38. **Oshiro, N., Y. Fukata, and K. Kaibuchi.** 1998. Phosphorylation of moesin by rho-associated kinase (rho-kinase) plays a crucial role in the formation of microvilli-like structures. J. Biol. Chem. **273:**34663–34666.
39. **Parsons, J. T.** 1996. Integrin mediated signaling: regulation by tyrosine kinases and small GTP-binding proteins. Curr. Opin. Cell Biol. **8:**146–152.

40. **Pleiman, C. M., W. M. Hertz, and J. C. Cambier.** 1994. Activation of phosphatidylinositol-3′ kinase by Src-family kinase SH3 binding to the p85 subunit. Science **263:**1609–1612.
41. **Plow, E. F., T. A. Haas, L. Zhang, J. Loftus, and J. W. Smith.** 2000. Ligand binding to integrins. J. Biol. Chem. **275:**21785–21788.
42. **Poullet, P., A. Gautreau, G. Kadare, J. A. Girault, D. Louvard, and M. Arpin.** 2001. Ezrin interacts with focal adhesion kinase and induces its activation independently of cell-matrix adhesion. J. Biol. Chem. **276:**37686–37691.
43. **Renne, R., D. Blackbourn, D. Whitby, J. Levy, and D. Ganem.** 1998. Limited transmission of Kaposi's sarcoma-associated herpesvirus in cultured cells. J. Virol. **72:**5182–5188.
44. **Ridley, A. J.** 2001. Rho proteins: linking signaling with membrane trafficking. Traffic **2:**303–310.
45. **Russo, J. J., R. A. Bohenzky, M. C. Chien, J. Chen, M. Yan, D. Maddalena, J. P. Parry, D. Peruzzi, I. S. Edelmen, Y. Chang, and P. S. Moore.** 1996. Nucleotide sequence of the Kaposi's sarcoma-associated herpesvirus (HHV-8). Proc. Natl. Acad. Sci. USA **93:**14862–14867.
46. **Sastry, S. K., and K. Burridge.** 2000. Focal adhesions: a nexus for intracellular signaling and cytoskeletal dynamics. Exp. Cell. Res. **261:**25–36.
47. **Schaller, M. D.** 2001. Biochemical signals and biological responses elicited by the focal adhesion kinase. Biochim. Biophys. Acta **1540:**1–21.
48. **Schlaepfer, D. D., and T. Hunter.** 1997. Focal adhesion kinase overexpression enhances ras-dependent integrin signaling to ERK2/mitogen-activated protein kinase through interactions with and activation of c-Src. J. Biol. Chem. **272:**13189–13195.
49. **Schlaepfer, D. D., C. R. Hauck, and D. J. Sieg.** 1999. Signaling through focal adhesion kinase. Prog. Biophys. Mol. Biol. **71:**435–478.
50. **Schulz, T. F., J. Sheldon, and J. Greensill.** 2002. Kaposi's sarcoma-associated herpesvirus (KSHV) or human herpesvirus 8 (HHV-8). Virus Res. **82:**115–126.
51. **Schulz, T. F., Y. Chang, and P. S. Moore.** 1998. Kaposi's sarcoma-associated herpesvirus (human herpesvirus 8), p. 87–134. *In* D. J. McCance (ed.), Human tumor viruses. ASM Press, Washington, D.C.
52. **Takeda, H., T. Matozaki, T. Takada, T. Noguchi, T. Yamao, M. Tsuda, F. Ochi, K. Fukunaga, K. Inagaki, and M. Kasuga.** 1999. PI-3K gamma and protein kinase C-zeta mediate RAS-independent activation of MAP kinase by a Gi protein-coupled receptor. EMBO J. **18:**386–395.
53. **Tapon, N., and A. Hall.** 1997. Rho, Rac, Cdc42 GTPases regulate the organization of the actin cytoskeleton. Curr. Opin. Cell Biol. **9:**86–92.
54. **Thomas, J. W., B. Ellis, R. J. Boerner, W. B. Knight, G. C. White, and M. D. Schaller.** 1998. SH2- and SH3-mediated interactions between focal adhesion kinase and Src. J. Biol. Chem. **273:**577–583.
55. **Triantafilou, K., Y. Takada, and M. Triantafilou.** 2001. Mechanisms of integrin-mediated virus attachment and internalization process. Crit. Rev. Immunol. **21:**311–322.
56. **Vieira, J., O. Hearn, L. E. Kimball, B. Chandran, and L. Corey.** 2001. Activation of KSHV (HHV-8) lytic replication by human cytomegalovirus. J. Virol. **75:**1378–1386.
57. **Virji, M.** 1996. Microbial utilization of human signaling molecules. Microbiology **142:**3319–3336.
58. **Wang, F. Z., S. M. Akula, N. S. Walia, L. Zeng, and B. Chandran.** 2003. Human herpesvirus 8 envelope glycoprotein B mediates cell adhesion via its RGD sequence. J. Virol. **77:**3131–3147.
59. **Wang, F.-Z., S. M. Akula, N. P. Pramod, L. Zeng, and B. Chandran.** 2001. Human herpesvirus 8 envelope glycoprotein K8.1A interaction with the target cells involves heparan sulfate. J. Virol. **75:**7517–7527.
60. **Wilde, A., E. C. Beattie, L. Lem, D. A. Riethof, S. H. Liu, W. C. Mobley, P. Soriano, and F. M. Brodsky.** 1999. EGF receptor signaling stimulates SRC kinase phosphorylation of clathrin, influencing clathrin redistribution and EGF uptake. Cell **96:**677–687.
61. **Wu, C., A. E. Chung, and J. A. McDonald.** 1995. A novel role for $\alpha 3\beta 1$ integrins in extracellular matrix assembly. J. Cell Sci. **108:**2511–2523.
62. **Zhu, L., V. Puri, and B. Chandran.** 1999. Characterization of human herpesvirus-8 K8.1 A/B glycoproteins by MAb. Virology **262:**237–249.